Radar Based Estimation of Ditches in the Vicinity of the Road

Christopher Dahlin Rodin

LUND UNIVERSITY

Department of Automatic Control

MSc Thesis
ISRN LUTFD2/TFRT--5970--SE
ISSN 0280-5316

Department of Automatic Control
Lund University
Box 118
SE-221 00 LUND
Sweden

Printed in Sweden by Tryckeriet i E-huset
Lund 2015

Abstract

Radars used for detecting objects with a positive elevation, such as other vehicles, are common in autonomous parking and braking systems in modern vehicles. Detecting objects with a negative elevation, such as ditches and holes, is however more troublesome. A common approach is to use a lidar, but a lidar is very costly and fragile compared to a radar. In this thesis, two two-dimensional radars are attached above the windshield of a truck and aimed down towards the ground.

At first the geometrical limitations of detecting ditches is analyzed in order to find which mounting angles of the radars are viable. Data is then collected from the radars, with the determined angles, a Global Positioning System (GPS) unit, and Inertial Measurement Unit (IMU) by driving the truck in a real world terrain. Data from a lidar is also recorded for reference.

Combined with a GPS and IMU, the radar detections are first transformed from the radar coordinate system, the a truck coordinate system, and finally to global Universal Transverse Mercator (UTM) coordinates. The global position of each detection is filtered, and finally used to create an elevation map of the environment. A similar map is also created from the lidar detections.

The resulting radar elevation map accurately maps the terrain near the vehicle, including the ditches next to the road. The radars appear to miss small objects, and the density of the detections is quite low for the radar mount angles used.

In order to improve the accuracy, the vertical position of the radar detection needs to be determined. A higher density of detections would also improve the mapping, which could be aquired by decreasing the pitch angle of the radars.

Acknowledgements

The project described in this thesis was carried out at the department of Advaned Driver Assistance Systems at Scania CV AB in Södertälje, Sweden, where my my main supervisor was Kristian Lundh. Kristian has not only guided me through the formalities required for carrying out all the work and experiements, but even more so motivated and supported me when I encountered problems. I can not thank Kristian enough for all the time he has spent doing this, especially considering the busy schedule of the department.

Lars Hjort and Marco Trincavelli have been my informal supervisors at Scania, and have helped me greatly with both their theoretical expertise and experience in carrying out projects. I am also very grateful for the support I have received from all the other members at the department, and the welcoming atmosphere they all have provided.

I would also like to thank the head of the department, Jon Andersson, for motivating me with both his enthusiastic presentations and his interest in my work.

I am also very thankful for both the guidance through academic formalities and the supporting environment provided by the department of Automatic Control at Lund University, in particular from my supervisor professor Bo Bernhardsson.

Finally I would like to thank all the other thesis workers whom I have encountered at Scania, the days would have passed much slower if it were not for you.

Contents

1

Introduction

This work aims to investigate the feasability of detecting ditches in the vicinity of the road using two two-dimensional radars, and a High Performance Inertial Measurement Unit and Global Positioning System (HPIG). The project was carried out at the department of Advanced Driver Assistance Systems at Scania CV AB in Södertälje, Sweden. This chapter contains the background for the project, what has previously been done, the goals and limitations of the project, and finally how the project was carried out.

1.1 Background

Road transportation only needs a road for the vehicle to drive on, making it a cheap and in many aspects the most flexible mode of transport. This has lead to road transportation becoming the most used mode of transport within the European Union, accounting for 45 % of goods transport in 2012 [European Commission, 2014]. The flexibility, large amount of objects on the roads, and high diversity of objects on the roads - trucks, cars, cyclists, pedestrians, and even animals - creates a highly dynamic environment, making it difficult to avoid accidents and consistently drive at speeds that minimize fuel consumption.

Within the European Union, close to thirty thousand people were killed in accidents on roads in 2012. Compared to rail and air transport, road traffic fatalities are highly overrepresented both in absolute numbers and fatalities per person-kilometer and ton-kilometer [European Commission, 2014]. With human errors being contributing factor in nine out of ten road traffic accidents [Forward, 2008], considerably higher than both vehicle faults and environmental factors, active safety systems has become one of the focus areas when improving vehicle safety. Early active safety systems such as traction control and brake assist has been developed and implemented during the last decades, and with the ongoing development of intelligent vehicles, even more safety risks can be handled faster each year [Cheng, 2011].

If the current proven technologies - such as chosing the most fuel-efficient route - are implemented at a slow and steady pace, the fuel consumption can be reduced by over 6 % within 10 years [Shaw, 2013]. This will be an important contribution for reaching climate and energy targets set up by the European Union amongst others, and if future technologies are taken into account the fuel savings can be even larger.

All the benefits of letting computers handle the operation of vehicles has lead to the rapid research and development of intelligent vehicles. An intelligent vehicle is a vehicle which can drive autonomously, either fully or partly. The purpose of intelligent vehicles can be to increase safety, comfort, and energy efficiency [Cheng, 2011].

To achieve a high level of autonomy the intelligent vehicle needs to be able to both localize itself within a map, and create or update the map in real-time to account for changes in the environment. The localization can be done very accurately by a high precision Global Positioning System (GPS) and mapping by a Light Detection and Ranging (lidar) system. However, these high precision sensors are very costly and there are still questions about their mechanical robustness due to moving parts [Ozguner et al., 2011]. Another way to solve the problem of localization and mapping is to use a pre-existing map and use sensors to identify known terrain characteristics. The position of the vehicle can then be found by comparing the position of the terrain characteristics in relation to the vehicle to their position in the map, which removes the need for a high precision GPS. Cheaper and more robust sensors could also be used to identify terrain characteristics, such as a radar.

1.2 Previous Work

Radars have been in use in a number of applications since their introduction in the 20th century, not least in military and meterological applications [Skolnik, 2008]. The use of radars in road traffic vehicles however is fairly new, but is quickly growing. Radars used to detect objects above the ground level are already in place in commersial vehicles, where they are used for assisted braking and parking [Jain and Heydari, 2012].

NASA's jet propulsion laboratory suggested a method of detecting ditches by using a continuous-wave radar and exploiting diffraction to see around the corners of the ditch [Mittskus and Lux, 2006]. This could be an alternative method of detecting ditches, and is fundamentally a different approach than the method in this project.

There has also been work done in detecting ditches using the combination of a stereo camera and a long range radar [Agnew, 2014]. This method focuses on detecting holes in the road in front of the vehicle, which makes its use more spe-

cialized and limited.

There has been much work done in general mapping and ditch detection using more advanced sensors, in particular lidars. This has been done very successfully since lidars can locate objects with a very high accuracy. Lidars are currently very expensive and do not function well in rough weather condutions such as rain and fog [Vlacic, 2009]. This makes it interesting to investigate the feasability to use radars to detect ditches.

1.3 Goals and Limitations

This project aims to explore the possibility of using two radars aimed towards the ground to obtain information which can be used in intelligent vehicle functions, such as brake assist and localization and mapping. See figure 1.1 for a sketch of the radar position on the truck. More specifially, the radars will be used to identify objects. Since most objects above the ground can already be detected by existing radars the focus will be on ditches, but the possibility of detecting objects above the groud which are currently not identifiable will also be analyzed.

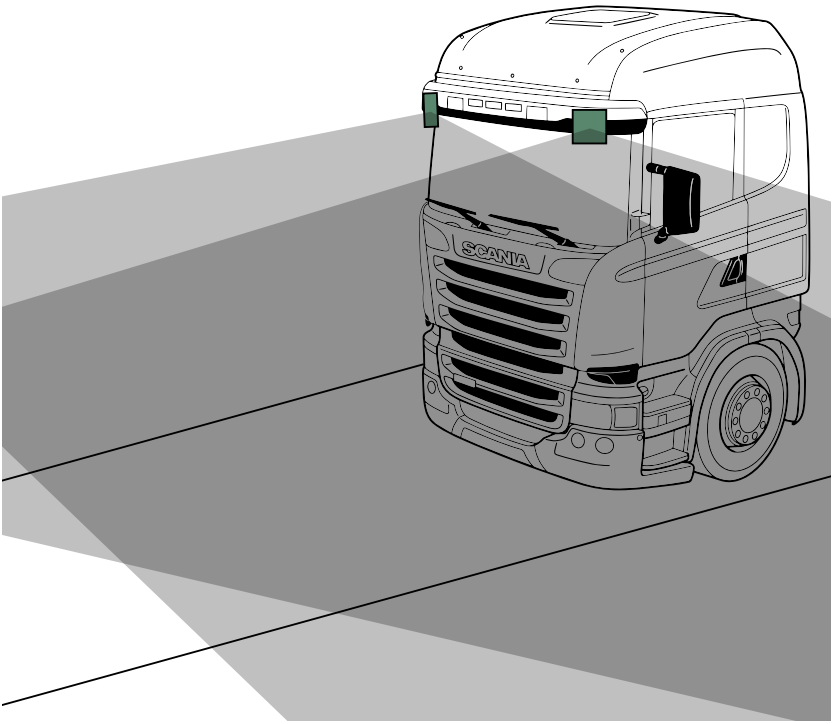

Figure 1.1 The general idea of the project - two radars mounted above the windshield of a truck, aimed down towards the ground. The shadowed area represents the radar beams. © Scania CV AB

The general goal can be breaken down into two parts. The first is to find the theoretical limits of detecting ditches, which will take into account the geometry of the ditches and radar beam. The second is to find the practical limits of detecting ditches, which will be done through experiments, and mapping the environment.

As can be seen in details in the report, the exact pose of the radars needs to be determined to find the exact position of the target. This project takes into account the mount position and angle of the sensors on the truck, as well as the current pose of the truck in the global coordinate system. To fully utilize the precision of the radars, the movement of the truck cabin relative to the truck needs to be taken into account. Unfortunately sensors required for this are not available for the project, and the truck cabin movements will not be taken into account.

1.4 Methodology

The project was initiated with a literature study to obtain an overview of what previously had been done in the area of ditch detection, and which methods could potentially be used. A major part of the preparations was also to become familiar with the platform - the truck and all the sensors - and the simulation environment used at Scania.

The radars were mounted early on with unknown angles which were then measured, and some data was aquired to analyze how much information is possible to retrieve, and to develop software to transform the data from the radar to three-dimensional positions and radial velocities.

In order to find out how well the radars theoretically can detect different types of objects, the theoretical limits were calculated numerically for positive objects - objects with a positive height, such as poles and hills - and negative objects - objects with a negative height, such as holes and ditches - using simple geometrical models.

Finally the radars were adjusted to, as close as possible, obtain the calculated optimal roll, pitch, and yaw angles. The experiment described in the report was then carried out, and the data was analyzed to find out how well it is possible to detect dithes and creating a consistent map of the environment.

The work flow of the practical moments in the projects are shown in figure 1.2.

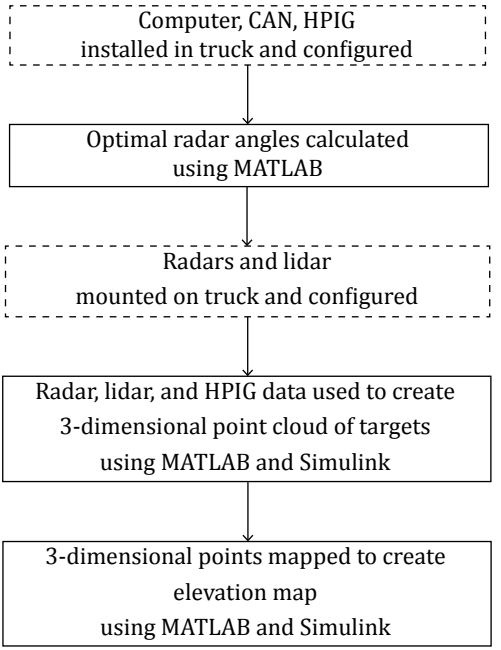

Figure 1.2 The work flow of the practical moments in the projects. The full drawn boxes show tasks performed by me, and dashed boxes show tasks performed by other people at Scania.

2

Platform

The platform consists of a truck with variety of sensors attached. The sensors are connected to a unit with enough computing power to run several intelligent vehicle functions, such as path planning and object detection, in real time. In this chapter the truck and the sensors used are described in detail. The sensors used in this project is the High Performance Intertial Measurement Unit and Global Positioning System (HPIG) and two radars. A lidar is used for reference but not in the ditch detection system itself.

2.1 Truck

The truck used in this project is the Scania test truck named Astator, which is a modified Scania truck with a G480 cab. A photo of the truck can be seen in figure 2.1. Astator contains all the required equipment to both gather data from the sensors, and use the data to run several intelligent functions in real time such as mapping, path planning, and vehicle control.

Figure 2.1 The Scania test truck Astator used in this project. © Scania CV AB

As is common for trucks, there is a suspension between the cab and frame. This means that the cab can move several centimeters relative to the frame, and can have a quickly changing velocity [Marcu, 2009].

2.2 High Performance IMU and GPS

The High Performance Inertial Measurement Unit and Global Positioning System (HPIG) is a sensor combining a high performance Intertial Measurement Unit (IMU, see [Mostafa and Hutton, 2001] for a detailed explanation of the sensor) and Global Positioning System (GPS, see [Xu, 2007] for a detailed explanation of the sensor). The IMU is a standard sensor widely used in Scania trucks, and measures the three-dimensional orientation (roll, pitch, and yaw angles), the orientation angular velocities, and the positional acceleration in a three-dimensional cartesian coordinate system. The GPS measures the global position of the HPIG, and is much more accurate than the standard GPS. Since the accuracy makes the GPS very costly, it is unsuitable for production vehicles. However, it makes sense to use a high precision GPS in this project to remove the effects of inaccurate global positioning.

Measurements

The HPIG is used to measure both the positional and inertial quantities of the truck. The position obtained directly from the HPIG is in World Geodetic System 1984 (WGS84, see [Xu, 2007] for a more detailed explanation), but is preprocessed with

filters and converted to the Universal Transverse Mercator (UTM, see [Dutch, 2014] for a more detailed explanation) coordinate system. The quantities used in this project are summarized in table 2.1.

Property	Annotation	Quantity	Unit
x position in UTM	x_{hpig}	-	m
y position in UTM	y_{hpig}	-	m
Altitude above mean sea level	z_{hpig}	-	m
Position standard deviation	σ_{hpig}	0.02	m
Velocity	$\overrightarrow{v}_{\text{hpig}}$	-	m/s
Roll	$\theta_{\text{hpig roll}}$	-	°
Pitch	$\theta_{\text{hpig pitch}}$	-	°
Yaw	$\theta_{\text{hpig yaw}}$	-	°
Roll standard deviation	$\sigma_{\text{hpig roll}}$	0.05	°
Pitch standard deviation	$\sigma_{\text{hpig pitch}}$	0.05	°
Yaw standard deviation	$\sigma_{\text{hpig yaw}}$	0.1	°
Roll rate	$\dot{\theta}_{\text{hpig roll}}$	-	° / s
Pitch rate	$\dot{\theta}_{\text{hpig pitch}}$	-	° / s
Yaw rate	$\dot{\theta}_{\text{hpig yaw}}$	-	° / s

Table 2.1 Summary of the quantities measured by the HPIG.

Mount

The HPIG unit is mounted inside the truck. The exact location is described in table 2.2 and visualized in figure 2.2.

Property	Annotation	Quantity	Unit
HPIG to rear axle	Δx_{hpig}	5.076	m
HPIG to centerline	Δy_{hpig}	0.000	m
HPIG to ground	Δz_{hpig}	1.770	m

Table 2.2 Summary of the mount position the HPIG.

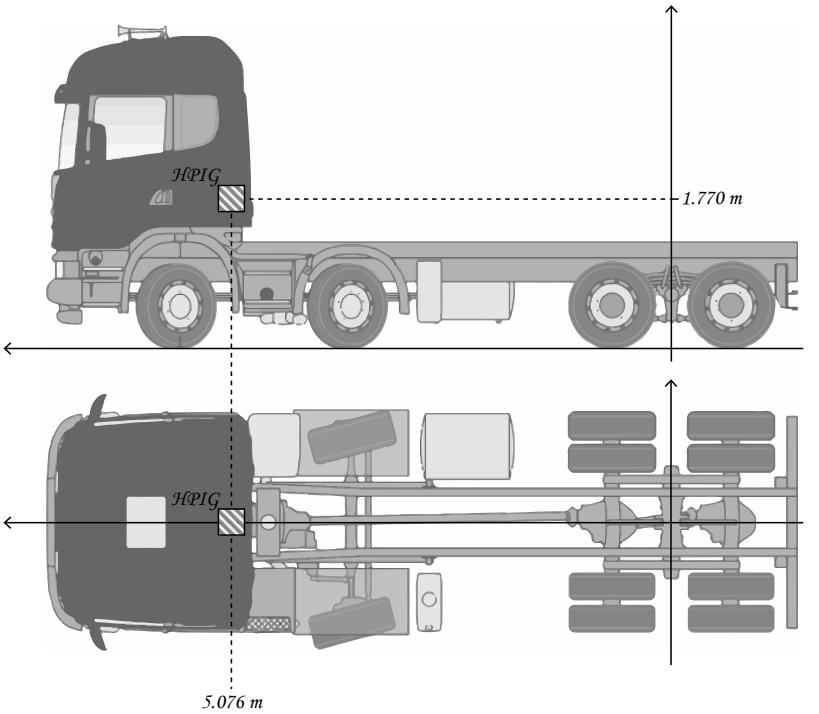

Figure 2.2 The position of the HPIG unit on the truck. © Scania CV AB

2.3 Radars

The main sensors used in this project are the radars. Radar is an acronym for RAdio Detection And Ranging, and is a system which uses radio waves to determine the range between the radar and an object [Skolnik, 2008]. The radar type used in this project - monopulse doppler radar - can also detect the radial velocity of the target, and the angle between the radar look angle and the target.

Operational Details

The radar first transmits radio waves with a known frequency. These waves propagates through the medium until they hit an object, and are then reflected away from the object. When the reflected radio wave reaches the radar again, the radar measures several characteristics of the reflected wave to find the range, radial velocity, and the angle between the radar look angle and the target. See figure 2.3 for a visual description of radar operation.

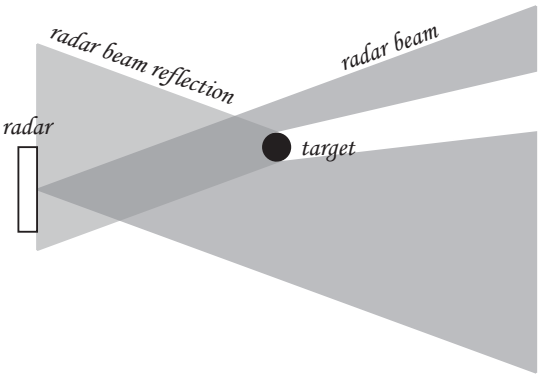

Figure 2.3 The basic operation of a radar. The radar beam travels from the radar, reaches the target, gets reflected, and finally reaches the radar again.

The range R between the radar and the target can be calculated from the time it takes for the radio wave to return to the radar [Levanon and Mozeson, 2004]:

$$R = c \cdot \frac{t_{\text{round trip}}}{2} \tag{2.1}$$

where $t_{\text{round trip}}$ is the time it takes for the radio wave to return to the radar, and c is the speed of light in the medium.

A doppler radar also takes into account the doppler effect to calculate the radial velocity - the component of the velocity pointing away from the radar - of the target [Skolnik, 2008]. The doppler effect states that there is a frequency shift in a wave transmitted from a source if the source is moving relative to the observer. The frequency of the received wave f_{r} is given by

$$f_{\text{r}} = f_{\text{t}} \frac{c + \dot{R}}{c - \dot{R}} \tag{2.2}$$

where f_{t} is the frequency of the transmitted wave and $\dot{R}$ is the range velocity of the target.

In practical applications it can be easier to find the frequency difference between the transmitted and received wave, called the doppler frequency. The doppler frequency f_{d} is given by

$$f_{\text{d}} = f_{\text{r}} - f_{\text{t}} = 2\dot{R} \frac{f_{\text{t}}}{c - \dot{R}} \tag{2.3}$$

If the radial velocity is much smaller than the speed of light in the medium, equation 2.3 can be simplified to obtain the radial velocity:

$$\dot{R} = \frac{c}{2}\frac{f_\mathrm{d}}{f_\mathrm{t}} \tag{2.4}$$

By transmitting the radio wave as a thin beam, with the angle between the beam and the radar look angle is known, the horizontal position of the target will be known. Since a thin beam creates a narrow horizontal field of view, the beam is transmitted several times with the direction of the beam going from one side to the other. This gives both an accurate position of each target and a wide horizontal field of view. The vertical position, however, is commonly unknown in two-dimensional radars. A visual description can be seen in figure 2.4. The propagation of the radar beams do not cut off as abruptly as in the figure, and is commonly defined as the region where the power greater than half the power (-3 dB) of the center of the beam [Melvin and Scheer, 2013].

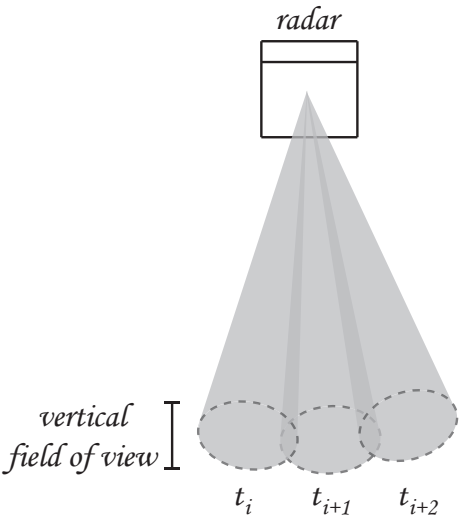

Figure 2.4 The radar beams transmitted by the radar to determine the horizontal field of view. The vertical field of view is unknown in the radars used in this project.

Measurements

The software for acquiring the signals was already in place, so the range, range velocity, and angle for each target could be obtained directly. The radars have a sample time of 50 ms and can acquire data for up to 64 detections per sample. The specification of the measured radar quantities can be seen in table 2.3.

Property	Annotation	Quantity	Unit
Range	R	-	m
Minimum range	R_{min}	0.5	m
Maximum range	R_{max}	85	m
Range standard deviation	σ_R	0.25	m
Radial velocity	$\dot{R}$	-	m/s
Radial velocity standard deviation	$\sigma_{\dot{R}}$	0.1	m/s
Angle	θ	-	°
Minimum angle	θ_{min}	-75	°
Maximum angle	θ_{max}	75	°
Angle standard deviation	σ_θ	1	°

Table 2.3 Summary of the quantities measured by the radars.

Mount

The radars are mounted above the windshield of the truck, and the exact position is described in table 2.4 and visualized in figure 2.5. The reasoning behind the mount angles can be found in section 4.2, and standard deviation in section 4.3. See section 3.1 for an explanation of the roll, pitch, and yaw angles.

Property	Annotation	Quantity	Unit
Left radar to rear axle	$\Delta x_{\text{radar left}}$	6.907	m
Left radar to centerline	$\Delta y_{\text{radar left}}$	0.770	m
Left radar to ground	$\Delta z_{\text{radar left}}$	2.750	m
Left radar roll	$\theta_{\text{radar left roll}}$	11	°
Left radar pitch	$\theta_{\text{radar left pitch}}$	-35	°
Left radar yaw	$\theta_{\text{radar left yaw}}$	27	°
Right radar to rear axle	$\Delta x_{\text{radar right}}$	6.927	m
Right radar to centerline	$\Delta y_{\text{radar right}}$	0.770	m
Right radar to ground	$\Delta z_{\text{radar right}}$	2.760	m
Right radar roll	$\theta_{\text{radar right roll}}$	-8	°
Right radar pitch	$\theta_{\text{radar right pitch}}$	-27	°
Right radar yaw	$\theta_{\text{radar right yaw}}$	-16	°
Mount angle standard deviation	$\sigma_{\text{angle meas.}}$	1	°
Mount position standard deviation	$\sigma_{\text{pos. meas.}}$	0.05	m

Table 2.4 Summary of the mount positions and angles of the radars.

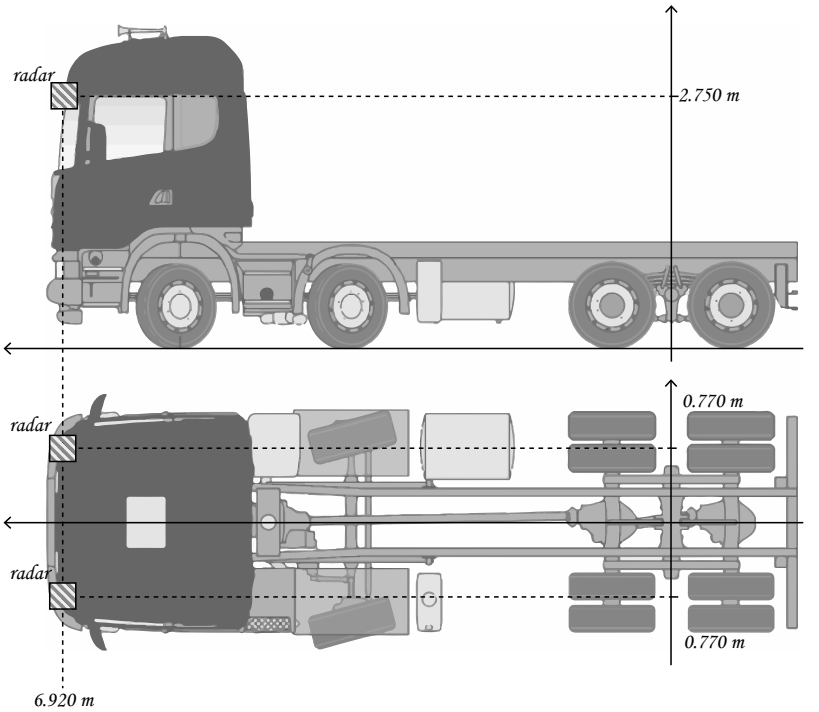

Figure 2.5 The position of the radars on the truck. © Scania CV AB

2.4 Lidar

The lidar is similar in function to the radar, but uses laser beams instead of radio waves to find the position of the target [Ozguner et al., 2011]. Automotive lidars have a higher precision than automotive radars, but are also more costly, and there are still questions regarding the mechanical robustness of lidars due to their moving parts [Ozguner et al., 2011]. The lidar in this project will therefore be used as a reference for the radar data, and not be included in the ditch detection system.

The lidar, like the radar, measures the range between the lidar and the target, and the angle between the lidar look angle and the target. Additionally, the lidar produces four layers each scan. The vertical field of view is 3.2°, and the layers are thus separated vertically by 3.2 / (4-1) $\approx$ 1.07°.

Measurements

The lidar data could be obtained directly as range, angle and layer. The lidar samples data with a period of 20 ms, and can detect up to 116 targets per layer and scan. The details of the quantities measured by the lidar are found in table 2.5.

Property	Annotation	Quantity	Unit
Range	R_{lidar}	-	m
Maximum range	$R_{\text{lidar max}}$	200 m	
Range accuracy	$R_{\text{lidar acc}}$	0.1	m
Angle	θ_{lidar}	-	rad
Minimum angle	$\theta_{\text{lidar min}}$	-50	°
Maximum angle	$\theta_{\text{lidar max}}$	35	°
Layer	l_{lidar}	-	-
Number of layers	$l_{\text{lidar n}}$	4	-

Table 2.5 Summary of the quantities measured by the lidar.

Mount

The lidar is mounted above the windshield of the truck, but slightly lower than the radars. The exact position of the lidar are described in table 2.6, and visualized in figure 2.6.

Property	Annotation	Quantity	Unit
Lidar to rear axle	$\Delta x_{\text{radar left}}$	7.012	m
Lidar to centerline	$\Delta y_{\text{radar left}}$	0.000	m
Lidar to ground	$\Delta z_{\text{radar left}}$	2.640	m
Lidar roll	$\theta_{\text{radar left roll}}$	0	°
Lidar pitch	$\theta_{\text{radar left pitch}}$	-31	°
Lidar yaw	$\theta_{\text{radar left yaw}}$	0	°

Table 2.6 Summary of the mount positions and angles of the lidar.

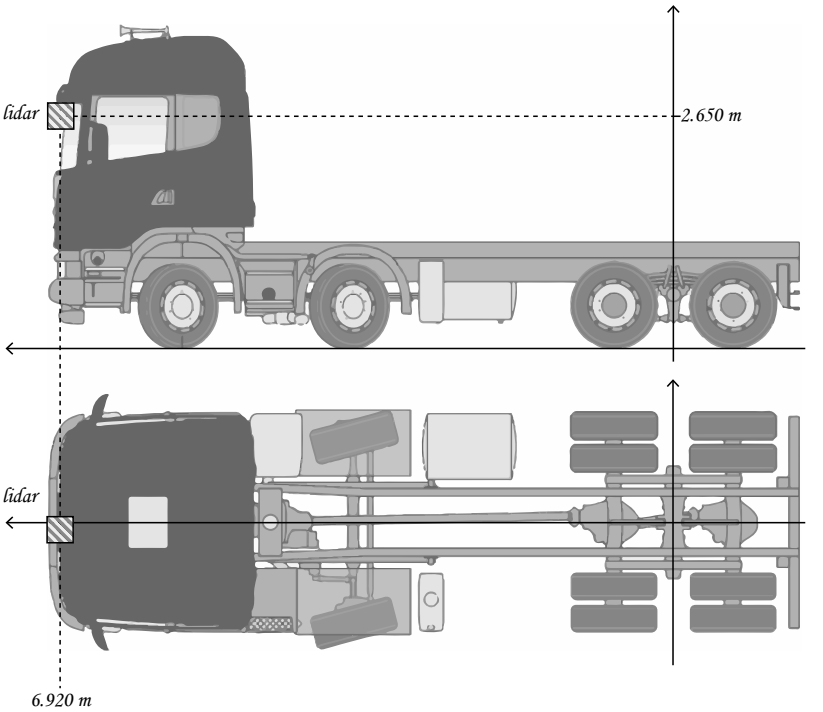

Figure 2.6 The position of the lidar on the truck. © Scania CV AB

3

Algorithms

This chapter contains the details of the data processing. At first the method of transforming sensor data to a global three-dimensional position and velocity is described. The method of filtering the data is then described, followed by an overview on how measurement deviations are calculated. Finally the method of creating an elevation map, and an estimation of certainty in the elevation map is described.

3.1 Geometry

Two-dimensional Formalism and Application

As described in section 2.3 about the radar operational details and section 2.4 about the lidar operation, the positioning of an object by the radars and lidar is obtained in range between the target and the radar, and angle between the radar or lidar look angle and the target. This type of coordinates are known as polar coordinates, which can be translated into two-dimensional cartesian coordinates according to equation 3.1 below. Figure 3.1 shows a visual description of the transformation.

$$\begin{bmatrix} x \\ y \end{bmatrix} = R \cdot \begin{bmatrix} \cos\theta \\ \sin\theta \end{bmatrix} \tag{3.1}$$

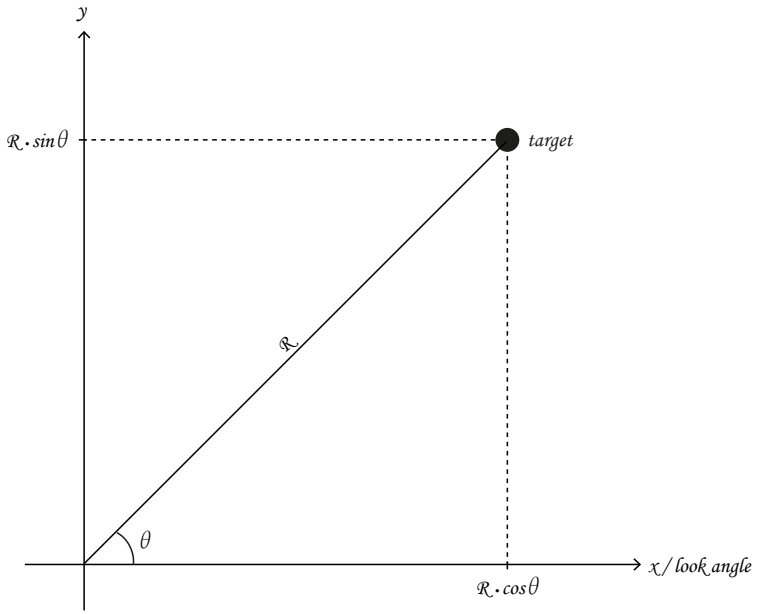

Figure 3.1 Transformation between polar coordinates and two-dimensional cartesian coordinates.

Three-dimensional Formalism

The pose of a coordinate system A in another coordinate system B is defined as the position and orientation of A in B [Diebel, 2006]. The position is simply the position of the origin of the first coordinate system in the other. The orientation is the angles of A in B. Figure 3.2 shows a coordinate system with an arbitrary pose in another coordinate system.

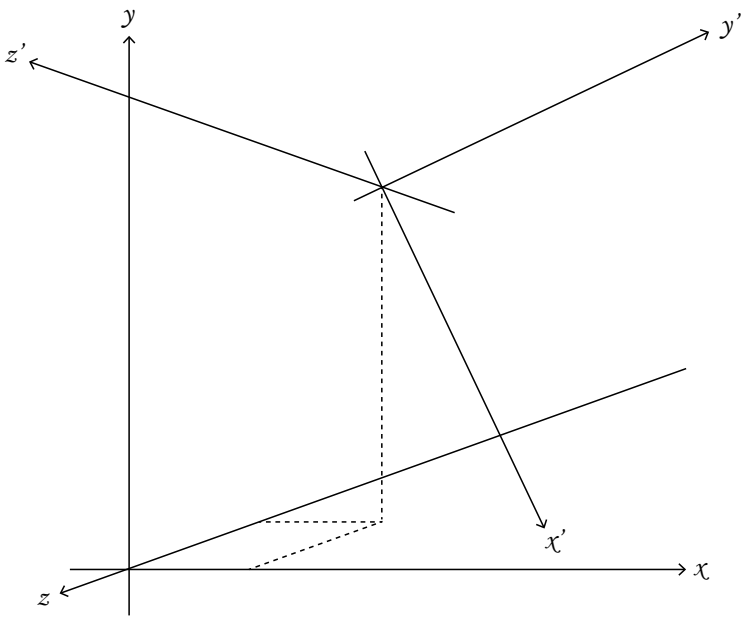

Figure 3.2 The coordinate system $x'y'z'$ in the coordinate system xyz. $x'y'z'$ is displaced and rotated compared to xyz, thus it has a different pose.

A common way of describing the orientation is with the Tait-Bryan angles - the rotation around the x-axis (roll), around the y-axis (pitch), and around the z-axis (yaw). An illustration of the roll, pitch, and yaw angles used in this project can be seen in figure 3.3.

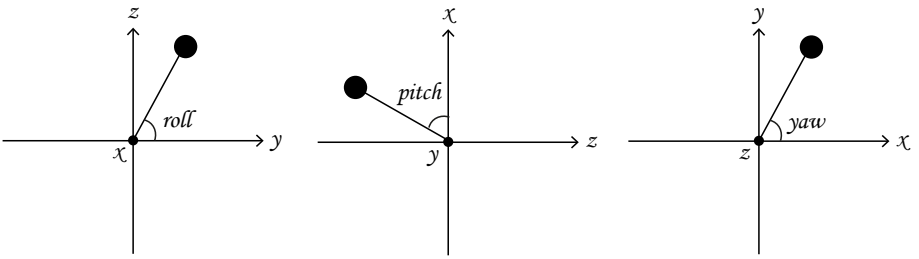

Figure 3.3 The definition of the roll, pitch, and yaw angles used in this project. The angles shown are in the positive direction.

Points can be translated from one three-dimensional coordinate system to another if its pose is known. The points are first rotated by multiplying them with a series of rotation matrices, where each rotation matrix rotates the point around one axis [Diebel, 2006]. The rotation matrices to rotate a point around the x-axis (roll), y-axis (pitch), and z-axis (yaw), are shown in equation 3.2, 3.3, and 3.4. The order which the rotation matrices are multiplied with the point to be translated represents the order of rotation, and is not commutative. When the rotations occur around fixed axes which do not change with the rotations, the rotations are called extrinsic.

$$\mathrm{R}_x(\theta) = \begin{bmatrix} 1 & 0 & 0 \\ 0 & cos\theta & -sin\theta \\ 0 & sin\theta & cos\theta \end{bmatrix} \tag{3.2}$$

$$\mathrm{R}_y(\theta) = \begin{bmatrix} cos\theta & 0 & -sin\theta \\ 0 & 1 & 0 \\ sin\theta & 0 & cos\theta \end{bmatrix} \tag{3.3}$$

$$\mathrm{R}_z(\theta) = \begin{bmatrix} cos\theta & -sin\theta & 0 \\ sin\theta & cos\theta & 0 \\ 0 & 0 & 1 \end{bmatrix} \tag{3.4}$$

After rotation, the points are displaced by the position of the origin of the first coordinate system in the other. Equation 3.5 shows the complete equation to translate from one coordinate system to another with different pose.

$$\begin{bmatrix} x' \\ y' \\ z' \end{bmatrix} = \mathrm{R}_z(\theta_{\text{yaw}})\mathrm{R}_y(\theta_{\text{pitch}})\mathrm{R}_x(\theta_{\text{roll}}) \begin{bmatrix} x \\ y \\ z \end{bmatrix} + \begin{bmatrix} \Delta x \\ \Delta y \\ \Delta z \end{bmatrix} \tag{3.5}$$

x', y', and z' are the coordinates of the transformed point; R_x, R_y, R_z the transformation matrices from equations 3.2, 3.3, and 3.4; θ_{roll}, θ_{pitch}, and θ_{yaw} the roll, pitch, and yaw angles of the first coordinate system in the other; x, y, and z the coordinates

of the point before transformation, and Δx, Δy, and Δz the position of the origin of the first coordinate system in the other.

Three-dimensional Application

To be able to easily relate the position of the truck, sensors, and targets to each other, all coordinates are translated to the global Universal Transverse Mercator (UTM) coordinate system. This is done by first translating all points to the truck coordinate system, and then translating them to the global coordinate system. The truck coordinate system is a three-dimensional cartesian coordinate system with positive x pointing towards the front of the truck, positive y towards the left, and positive z upwards. A visual description can be seen in figure 3.4.

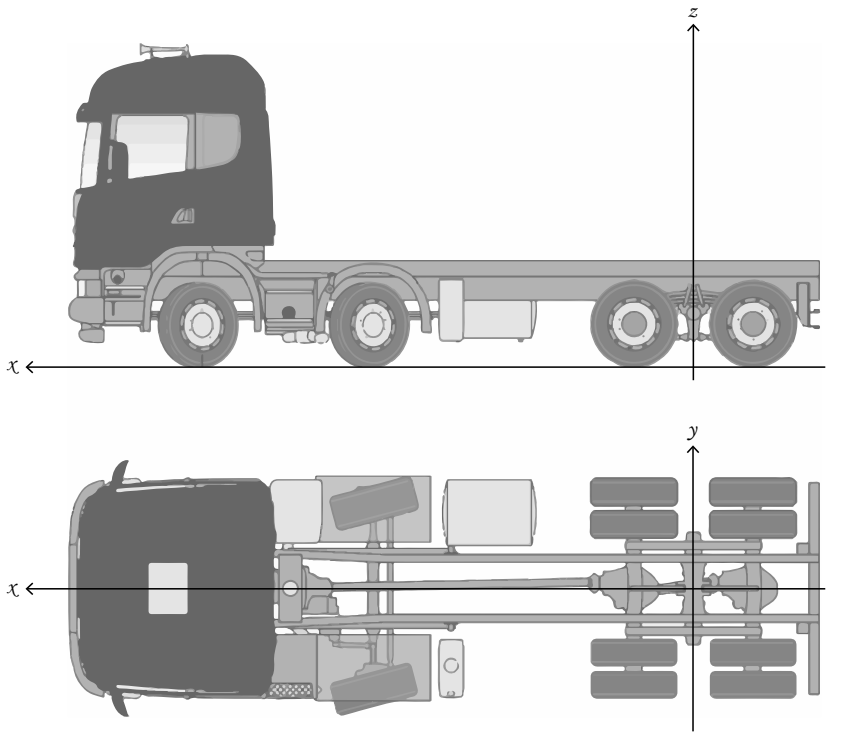

Figure 3.4 The truck coordinate system. The origin is on the ground below the back axis, positive x points towards the front of the truck, positive y towards the left side of the truck, and positive z upwards. © Scania CV AB

The coordinate systems of the sensors - the radars, lidar, and HPIG - have different poses than the truck coordinate system. The position and orientation are listed in

the corresponding sensor sections in chapter 2. After translating the radar and lidar detections from polar coordinates to cartesian coordinates according to equation 3.1, both the detections and sensor positions are translated to the truck coordinate system according to equation 3.5. The roll and yaw angles are simply the mount angles of the sensors, while the pitch is the sum of the mount pitch angle and vertical angle to the target, $\theta_{\text{lidar vertical}}$. With the vertical field of view $\theta_{\text{lidar vfov}}$, the number of layers, $n_{\text{lidar layers}}$, and the layer of the targets, l_{lidar}, known for the lidar, the vertical angle to the target can be calculated:

$$\theta_{\text{lidar vertical}} = \frac{l_{\text{lidar}}\theta_{\text{lidar vfov}}}{n_{\text{lidar layers}} - 1} - \frac{\theta_{\text{lidar vfov}}}{2} \tag{3.6}$$

For the radar there is no information about the vertical position of the target. However, with the radars being aimed towards the road, the radial velocity will be different for different vertical positions caused by different angles of incidence. If the quantities measured by the HPIG can be used to accurately model the velocity of the radar (see section 3.2), it is be possible to find the vertical position as the angle where the global velocity of the target is zero. The complete equations to calculate the position of a radar and lidar target in the truck coordinate system is then:

$$\begin{bmatrix} x_{\text{radar/lidar truck}} \\ y_{\text{radar/lidar truck}} \\ z_{\text{radar/lidar truck}} \end{bmatrix} = \mathrm{R}_{zyx} R_{\text{radar/lidar}} \begin{bmatrix} cos(\theta_{\text{radar/lidar}}) \\ sin(\theta_{\text{radar/lidar}}) \\ 0 \end{bmatrix} + \begin{bmatrix} \Delta x_{\text{radar/lidar}} \\ \Delta y_{\text{radar/lidar}} \\ \Delta z_{\text{radar/lidar}} \end{bmatrix} \tag{3.7}$$

where R_{zyx} is the rotation matrices from equation 3.2, 3.3, and 3.4:

$$\mathrm{R}_{zyx} = \mathrm{R}_z(\theta_{\text{radar/lidar yaw}})\mathrm{R}_y(\theta_{\text{radar/lidar pitch}} + \theta_{\text{radar/lidar vertical}})\mathrm{R}_x(\theta_{\text{radar/lidar roll}}) \tag{3.8}$$

Before translating the position of the radar and lidar targets to the global UTM coordinate system, the pose of the truck in UTM needs to be calculated. The UTM position and orientation is given by the HPIG, so equation 3.5 is used with the values in the values in table 2.1 and 2.2. Note that since the translation is from HPIG to truck coordinate system, negative Δx_{hpig}, Δy_{hpig}, and Δz_{hpig} are used. The complete equations for translating the HPIG UTM position to truck UTM position is given by equation 3.9

$$\begin{bmatrix} x_{\text{truck utm}} \\ y_{\text{truck utm}} \\ z_{\text{truck utm}} \end{bmatrix} = \mathrm{R}_z(\theta_{\text{hpig yaw}})\mathrm{R}_y(\theta_{\text{hpig pitch}})\mathrm{R}_x(\theta_{\text{hpig roll}}) \begin{bmatrix} -\Delta x_{\text{hpig}} \\ -\Delta y_{\text{hpig}} \\ -\Delta z_{\text{hpig}} \end{bmatrix} + \begin{bmatrix} x_{\text{hpig}} \\ y_{\text{hpig}} \\ z_{\text{hpig}} \end{bmatrix} \tag{3.9}$$

When the global position of the truck and the positions of the sensors and targets in the truck coordinate system are known, it is possible to calculate the global position of the targets and sensors, again with equation 3.5. The complete equations for translating targets from radar and lidar polar coordinates to global UTM coordinates are then given by equation 3.10.

$$\begin{bmatrix} x_{\text{radar/lidar utm}} \\ y_{\text{radar/lidar utm}} \\ z_{\text{radar/lidar utm}} \end{bmatrix} = \mathrm{R}_z(\theta_{\text{hpig yaw}})\mathrm{R}_y(\theta_{\text{hpig pitch}})\mathrm{R}_x(\theta_{\text{hpig roll}}) \begin{bmatrix} x_{\text{radar/lidar truck}} \\ y_{\text{radar/lidar truck}} \\ z_{\text{radar/lidar truck}} \end{bmatrix} + \begin{bmatrix} x_{\text{truck utm}} \\ y_{\text{truck utm}} \\ z_{\text{truck utm}} \end{bmatrix} \tag{3.10}$$

3.2 Kinematics

In order to calculate the vertical position of a target (see section 3.1) and filter out false detections (see section 3.4), the global velocity of an object needs to be determined. The velocity obtained from the radars is the radial velocity - the velocity away from or towards the radars. Since the radars are moving in the global coordinate system the radar velocity needs to be calculated in order to obtain the global velocity of the targets. The global velocity of the radars is the sum of the velocity of the truck in the global coordinate system, and the velocities caused by the angular velocities of the truck.

The forward and lateral velocity of the truck is measured by the HPIG, see table 2.1. There is no measurement for altitude velocity, but it can be estimated by calculating the change in altitude per second:

$$v_{\text{truck alt, i}} = \frac{v_{\text{truck z, i}} - v_{\text{truck z, i-1}}}{\text{HPIG sample time}} \tag{3.11}$$

A potential problem with this calculation is that since the altitude measurement by the HPIG occurs with a high frequency, a small error in the altitude measurement will result in a large error in the altitude measurement.

To obtain the truck velocity in the global UTM coordinate system, it is rotated around the truck origin by multiplying the yaw rotation matrix in equation 3.3 with the velocities:

$$\begin{bmatrix} v_{\text{truck x}} \\ v_{\text{truck y}} \\ v_{\text{truck z}} \end{bmatrix} = \mathrm{R}_z(\theta_{\text{hpig yaw}}) \begin{bmatrix} v_{\text{truck forw}} \\ v_{\text{truck lat}} \\ v_{\text{truck alt}} \end{bmatrix} \tag{3.12}$$

When the truck is driving on a rough surface or turning, the radars will gain tangential velocities proportional to the roll, pitch, and yaw angular velocities of the truck. The angular velocities are measured by the HPIG, and the tangential velocities $v_{\perp roll}$, $v_{\perp pitch}$, and $v_{\perp yaw}$ can be calculated as

$$v_{\perp\,\text{roll/pitch/yaw}} = d_{\text{roll/pitch/yaw}}\dot{\theta}_{\text{roll/pitch/yaw}} \tag{3.13}$$

where $d_{\text{roll/pitch/yaw}}$ is the distance between the radar and the axis which the rotation is occuring around:

$$d_{\text{roll}} = \sqrt{\Delta y_{\text{radar}}^2 + \Delta z_{\text{radar}}^2} \tag{3.14}$$

$$d_{\text{pitch}} = \sqrt{\Delta x_{\text{radar}}^2 + \Delta z_{\text{radar}}^2} \tag{3.15}$$

$$d_{\text{yaw}} = \sqrt{\Delta x_{\text{radar}}^2 + \Delta y_{\text{radar}}^2} \tag{3.16}$$

The global velocity of the radar is then given by

$$v_{\text{radar}} = v_{\text{truck}} + v_{\perp \text{ roll}} + v_{\perp \text{ pitch}} + v_{\perp \text{yaw}} \tag{3.17}$$

When the global velocity of the radar is known, the radial velocity in the direction of the target can be calculated by projecting the radar velocity vector onto a vector pointing from the radar to the target. A projection of the radar velocity vector, v_{radar}, onto the vector pointing from the radar to the target, $v_{\dot{R}}$, gives the component of v_{radar} that is in the direction of the target, $v_{\text{radar}/\dot{R}}$:

$$v_{\text{radar}/\dot{R}} = v_{\dot{R}} \frac{v_{\text{radar}} \cdot v_{\dot{R}}}{v_{\dot{R}} \cdot v_{\dot{R}}} \tag{3.18}$$

The global velocity of the target pointing away from or towards the radar is then given by:

$$v_{\text{target}} = v_{\text{radar}/\dot{R}} + v_{\dot{R}} \tag{3.19}$$

3.3 Measurement Errors

When measuring physical quantities, the measurement results will never be completely accurate due to the nature of measuring instruments [Rabinovich, 2005]. The measurement results will therefore always contain an error.

Error Distribution

In practical applications it is often difficult to know more than the general amplitude of the errors. For this state of knowledge it generally gives the best results to model the measurement as a normal distribution [Jaynes, 2003].

Equation 3.20 shows the probability density function (PDF) of the normal distribution, which evaluates the probability of a measurement to have the value x for a series of measurements with mean μ and standard deviation σ.

$$P(x) = \frac{1}{\sigma\sqrt{2\pi}} e^{-\frac{(x-\mu)^2}{2\sigma^2}} \tag{3.20}$$

The probability of a measurement to fall within an interval $[x_1, x_2]$ can then be calculated by integrating the EDF (3.20) from x_1 to x_2

$$P(\mu - x_1 \leq x \leq \mu + x_2) = \frac{1}{\sigma\sqrt{2\pi}} \int_{x_1}^{x_2} e^{-\frac{(x-\mu)^2}{2\sigma^2}} \, \mathrm{d}x \tag{3.21}$$

It is common to analyze the probability of a measurement falling within one, two, and three standard deviations from the mean. By evaluating equation 3.21 for those intervals, we obtain the values in table 3.1. See figure 3.5 for a graphical explanation.

Interval	Probability
$\mu \pm \sigma$	68.27%
$\mu \pm 2\sigma$	95.45%
$\mu \pm 3\sigma$	99.73%

Table 3.1 The probability of a measurement with a normally distributed error falling between one, two, and three standard deviations from the mean.

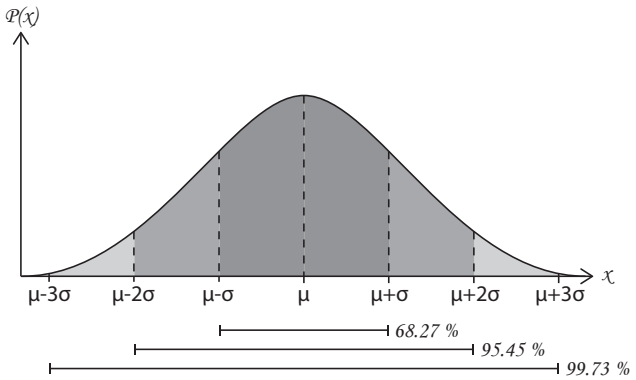

Figure 3.5 The PDF of normal distribution with the probability of a measurement falling between one, two, and three standard deviations from the mean shown as the area under the curve.

Error Propagation

In case the measurements are used to calculate another quantity, the measurement standard deviation needs to be re-calculated to obtain the standard deviation of the calculated quantity. For a function f which depends on the measurements x_1, x_2, ..., the standard deviation of f, σ_f, is calculated according to equation 3.22 [Ku, 1966].

$$\sigma_{f(x_1,x_2,\ldots)} = \sqrt{\left(\frac{\partial f}{\partial x_1}\right)^2 \sigma_{x_1}^2 + \left(\frac{\partial f}{\partial x_2}\right)^2 \sigma_{x_2}^2 + \ldots} \tag{3.22}$$

It can be interesting to calculate the standard deviation of the radar detections after the transformations to the global coordinate system. This can be done by applying equation 3.22 to the global coordinates calculation in equation 3.10. The standard deviations in the radar measurements, HPIG measurements, and the measured orientation and position of the radar on the truck is taken into account.

3.4 Filtering

When the radar beam reaches a target it gets reflected in multiple directions. If the reflected beam reaches another surface than the radar, gets reflected, and finally reaches the radar, the range, horizontal angle, and radial velocity will not have the correct values. Another source of interference in a multi-radar system is if one radar detects the reflections of a beam from another radar, which will also produce false values.

In order to remove the false detections caused by interference and double-bounces, the detections need to be filtered. Since the system is used to detect ditches and other terrain, only objects with no global velocity are of interest. The filter then simply removes detections with a velocity above a certain limit, v_{limit}, depending on how accurately it is possible to model the global velocity of the objects. The filter also removes detections with a range outside the interval $[R_{\min}, R_{\max}]$ and horizontal angle outside the interval $[\theta_{\min}, \theta_{\max}]$, which can be found in table 2.3.

3.5 Mapping

One way of representing the ditches and other terrain is an elevation map. An elevation map divides the terrain into squares and contains information about the elevation of each square. An illustration of an elevation map can be seen in figure 3.6.

Figure 3.6 An elevation map illustrated. The color shows the elevation of the square: blue indicates a higher elevation and red indicates a lower elevation. © Scania CV AB

When updating a square in an elevation map, the square of the detection first needs to be determined. If the elevation map is a two-dimensional matrix where each element represents a square where each side is 0.5 m, and the index of square $s_{i,j}$ is i, j, the indices i and j can be found according to

$$i = \left[\frac{x_{\text{radar/lidar utm}}}{s_{\text{size}}} \right] \tag{3.23}$$

$$j = \left[\frac{y_{\text{radar/lidar utm}}}{s_{\text{size}}} \right] \tag{3.24}$$

where the square brackets represents the closest integer to the value within them.

The elevation is then calculated from the radar or lidar detections in that square. There are several ways of calculating the elevation, which can take into account the standard deviation of the measurements. In this project the elevation is simply the average value of the detections in each square is used. The average value of each square, $e_{i,j}$, can be continuously updated after each new detection with the method for recursively calculating the average [Teknomo, 2006]:

$$e_{i,j\text{ new}} = \frac{c_{i,j} - 1}{c_{i,j}} e_{i,j\text{ previous}} + \frac{1}{c_{i,j}} z_{\text{radar/lidar utm}} \tag{3.25}$$

where $c_{i,j}$ is the number of detections in the square, and each square initially has the elevation zero.

It is of interest to know how much a square can be trusted. A square with several detections with little variance is more trustworthy than a square with only one detection or with a high variance. The number of detections in each square can be continuously updated by adding 1 each time a detection falls within a square. The variance of the detections within a square,$e_{i,j\ \sigma^2}$, can be continuously updated with the method for recursively calculating the variance [Teknomo, 2006]:

$$e_{i,j\ \sigma^2\ \text{new}} = \frac{c_{i,j}-1}{c_{i,j}} e_{i,j\ \sigma^2\ \text{previous}} + \frac{1}{c_{i,j}-1}(z_{\text{radar/lidar utm}} - e_{i,j\ \text{new}})^2 \tag{3.26}$$

where $c_{i,j}$ is the number of detections in the square, $e_{i,j\ \text{new}}$ the average elevation of the square, the initial variance of each square an arbitrary high number, and the variance of a square with only one detection is zero.

A block diagram of the full algorithm for updating a square after receiving a filtered detection from the radars or lidar can be seen in figure 3.7.

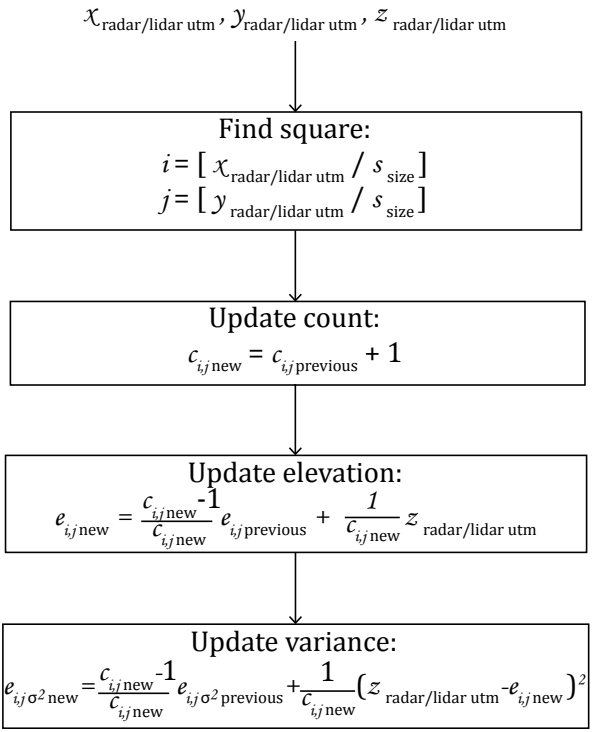

Figure 3.7 Block diagram describing the algorithm for updating a square in the elevation map after receiving a filtered detection from the radars or lidar.

4

Experimental Setup

In this chapter the preparations, measurements, and calculations used in the experiment is described. At first the possibilities of detecting positive and negative objects are analyzed. Then the optimal roll, pitch, and yaw angles for the radars are calculated for the chosen purposes, and combined with the mount limitations, the actual angles used for the experiment are determined. Finally the chapter contains and overview of the test track.

4.1 Geometrical Limitations

It is first important to find the geometrical limitations for detecting ditches in order to determine the optimal angles of the radars. To find the geometrical limitations, three types of objects are analyzed: positive objects not visible for radars already in place facing straight ahead, holes in the road, and ditches next to the road.

Range and Angle of Incidence

In order to create a detailed map, it is of high value to recieve many detections from the radars. If the angle of incidence of the radar beam to the ground is close to 0, there is a higher chance that the reflected beam will reach the radar. With the geometry of the radars in this project, a large angle of incidence also implies that the range between the radar and the detection is large, making it less likely for the radar to register a detection as the energy of the reflection is lower when it reaches the radar. This makes it interesting to analyze the largest range R at ground level, $z_{\text{radar truck}} = 0$ for different roll and pitch angles. Since a detection very far to the side is less interesting than a detection near the truck, only detections with $y_{\text{radar truck}}$ less than 5 meters away from the truck y_0 are analyzed in this section. The yaw angle is not analyzed since it only changes where the center of the radar beam is in relation to the truck, and do not affect the range.

At first the $z_{\text{radar truck}}$ is calculated from equation 3.7 and set to zero:

$$z_{\text{radar truck}} = \Delta z_{\text{radar}} + R(\cos\theta \sin\theta_{\text{pitch}} + \sin\theta \sin\theta_{\text{roll}} \cos\theta_{\text{pitch}}) = 0 \qquad (4.1)$$

Where θ is the horizontal angle measured by the radar. This equation is then solved for R:

$$R_{z=0}(\theta) = -\frac{\Delta z_{\text{radar}}}{\cos\theta \sin\theta_{\text{pitch}} + \sin\theta \sin\theta_{\text{roll}} \cos\theta_{\text{pitch}}} \tag{4.2}$$

The largest $R_{z=0}(\theta)$ for $y_{\text{radar truck}}$ within 5 meters of the truck y_0 for different roll and pitch angles are then found by numerically varying θ. When not varied, the roll is arbitrarily set to 10°, the pitch to -30°, and the yaw to 0°. The resulting diagrams can be seen in figure 4.1 and 4.3.

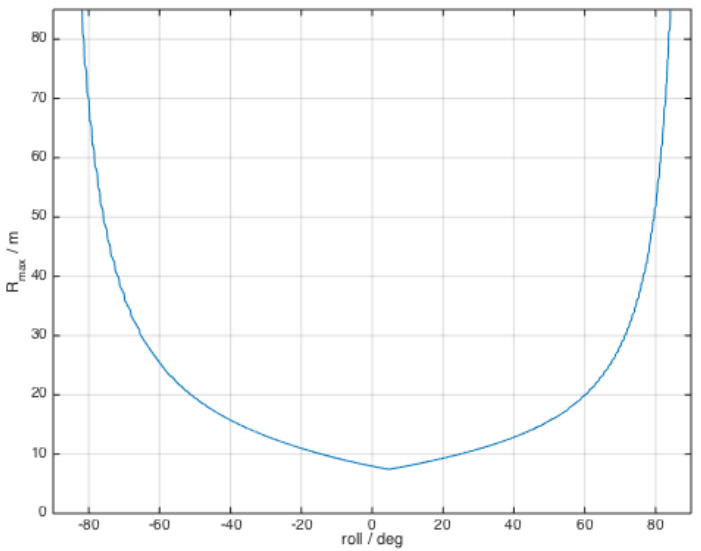

Figure 4.1 The maximum range between the radar and the radar beam on the ground for different roll angles, where the beam is not more than 5 meters away from the truck y_0.

It can be seen that the range increases as the absolute value of the roll angle increases. The minimun R_{max} is not at zero since the radar is not placed in the middle of the truck y wise. The increase in R is slow at first, and do not seem to cause a drastic increase in R_{max} until $\pm$ 35°. Another result of an increased roll angle is a narrower horizontal field of view, which is simply calculated according to equation 4.3 below. The corresponding diagram can be seen in figure 4.2.

$$\theta_{\text{horizontal fov}} = (|\theta_{\text{min}}| + |\theta_{\text{max}}|)\cos\theta_{\text{roll}} \tag{4.3}$$

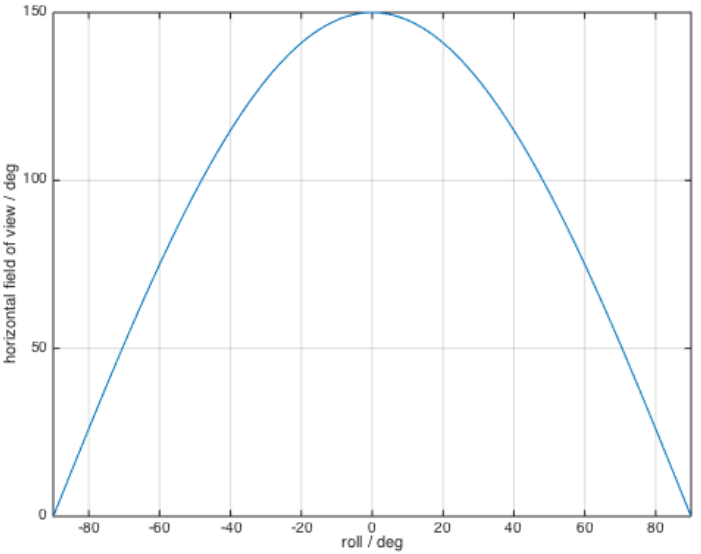

Figure 4.2 The horizontal field of view as a function of the roll angle of the radar.

The horizontal field of view decreases as expected with an increase in the roll angle. Similar to the R_{max}, the drastic decrease happens at around $\pm 35°$.

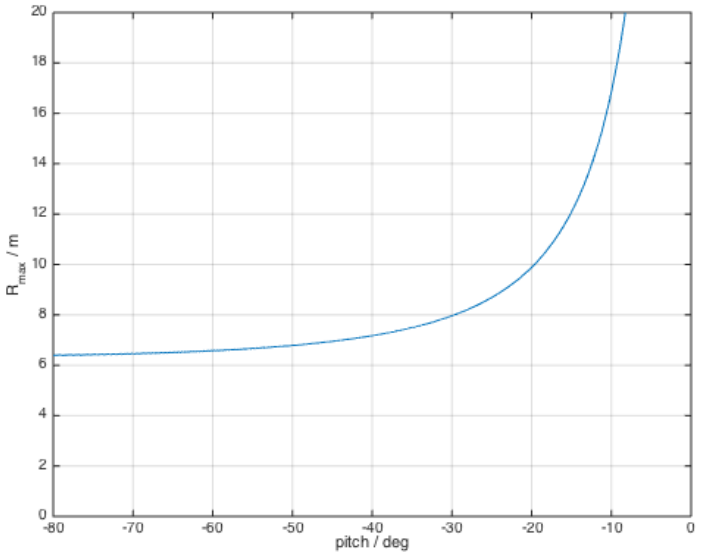

Figure 4.3 The maximum range between the radar and the radar beam on the ground for different pitch angles, where the beam is not more than 5 meters away from the truck y_0.

For the pitch, $R_{\max}$ increases slowly at first, and remains relatively low until the pitch reaches $-30°$.

Positive Objects

There are already methods in place which can map the environment in two dimensions, using radars rotated only in yaw - resulting in a beam which is parallel to the ground when driven on a flat surface. These methods can detect positive objects with a height depending on the mounting position of the radars.

A drawback of these methods is that they can not correctly detect the width of objects which are wider higher up, such as trees and certain fences. The focus will therefore be to detect positive objects with a height between 1 meter - the approximate mounting position of the current radars in height - and 3.5 meters - the approximate height of the truck.

To find out how high up the radars can see with different roll, pitch, and yaw angles, the maximum $z_{\text{radar truck}}$ is calculated for a point 1 meter next to the truck.

The $y_{\text{radar truck}}$ at this point is:

$$y_{\text{radar truck}} = \Delta y_{\text{radar}} \pm \left(\frac{w_{\text{truck}}}{2} + 1 \right) \tag{4.4}$$

Where w_{truck} is the width of the truck. By calculating $y_{\text{radar truck}}$ from equation 3.7, setting it equal to $y_{\text{radar truck}}$ in equation 4.4, the resulting equation can be solved for R:

$$R(\theta) = \frac{w_{\text{truck}}/2 + 1}{\sin\theta(\cos\theta_{\text{roll}}\cos\theta_{\text{yaw}} - \sin\theta_{\text{pitch}}\sin\theta_{\text{yaw}}) + \cos\theta\cos\theta_{\text{pitch}}\sin\theta_{\text{yaw}}} \tag{4.5}$$

To find the R and θ where $z_{\text{radar truck}}$ has its maximum, $z_{\text{radar truck}}$ is calculated from equation 3.7. Using the R from equation 4.5, the maximum $z_{\text{radar truck}}$ within the radar limits are found by varying the θ. The maximum $z_{\text{radar truck}}$ for different roll, pitch, and yaw can be seen in figure 4.4, 4.5, and 4.6 respectively. When not varied, the roll is arbitrarily set to 20°, the pitch to -30°, and the yaw to 30°.

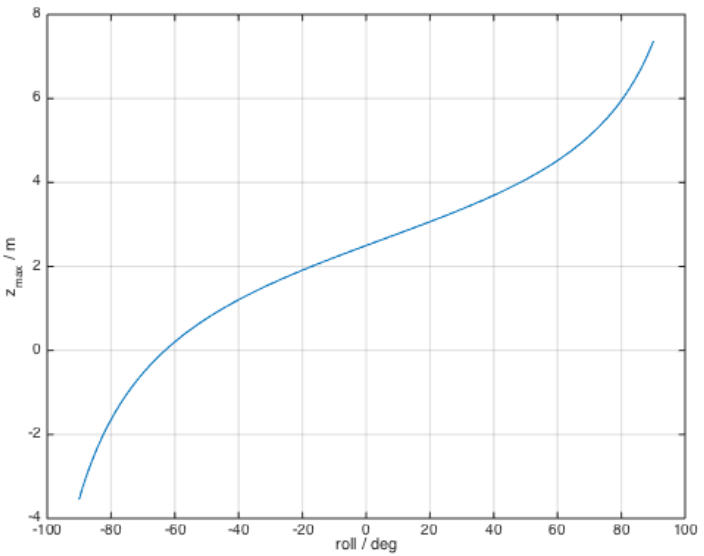

Figure 4.4 The maximum height the radar can see 1 meter beside the truck with varying roll angle.

It can be seen that a high roll angle makes it possible to see targets well above the truck. However, a high roll angle also gives a narrow horizontal field of view and a very varying range between the radar and the radar beam on the road, see

section 4.1. A roll of 35° is required for the radar to detect objects 3.5 meters above the ground. As discussed in section 4.1, this roll angle is acceptable, but close to too high.

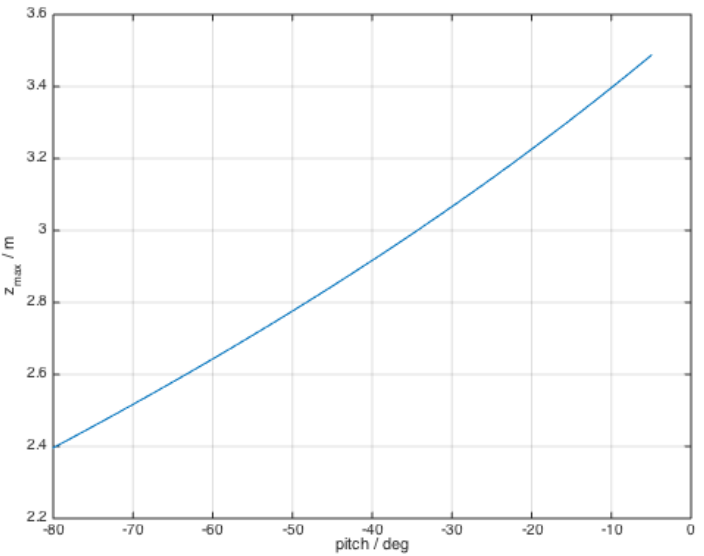

Figure 4.5 The maximum height the radar can see 1 meter beside the truck with varying pitch angle.

For the arbitrary angles and defined intervals, the radar beam reaches 3.5 meters above the ground when the pitch angle is larger than 5°. As discussed in section 4.1, a pitch angle larger than -30° causes a large distance between the radar beam on the ground, meaning that a pitch angle of -5° is not viable.

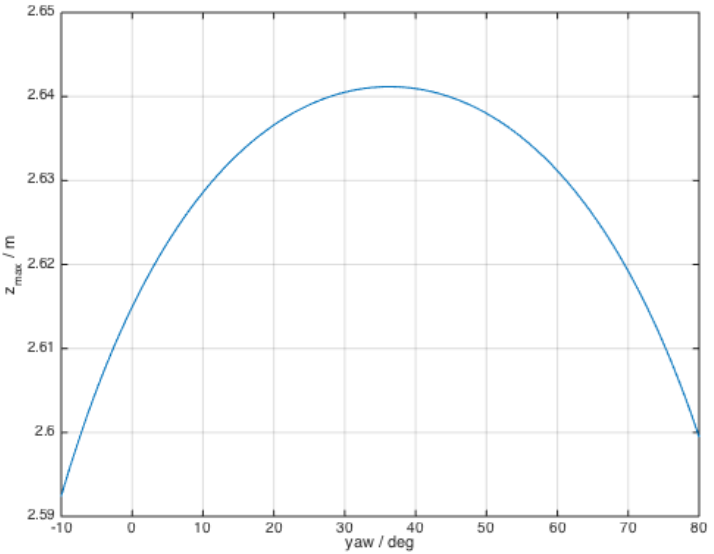

Figure 4.6 The maximum height the radar can see 1 meter beside the truck with varying yaw angle.

It can be seen that the yaw angle barely improves the ability of the radar to see objects high above the ground for the defined intervals.

As can be shown from varying the roll, pitch, and yaw angles, the roll angle is the only viable option when attempting to correctly detect objects which are high above the ground and near the truck. A suggested configuration for this can be seen in table 4.1. With this configuration, objects 3.5 above the ground can be correctly detected.

Angle	Value
roll	35°
pitch	-30°
yaw	30°

Table 4.1 A viable radar orientation for correctly mapping objects which are high above the ground and near the truck.

Holes in the Road

Objects with a negative height requires the radar beam to reach a certain depth in order to detect them properly. The depth that the radar beam reaches depends on the position and orientation of the radars on the truck, as well as the shape of the negative object.

If the angle of incidence on the road is too large, the radar beam will not be able to reach the full depth of the hole. This is illustrated in figure 4.7.

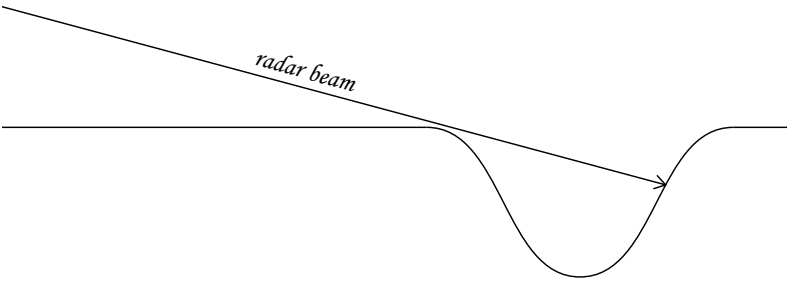

Figure 4.7 A sketch of how a radar beam can incorrectly detect the depth of a hole if the angle of incidence is too large.

The shape of a hole in the road is assumed to be circular with a depth proportional to a sine function, see figure 4.8.

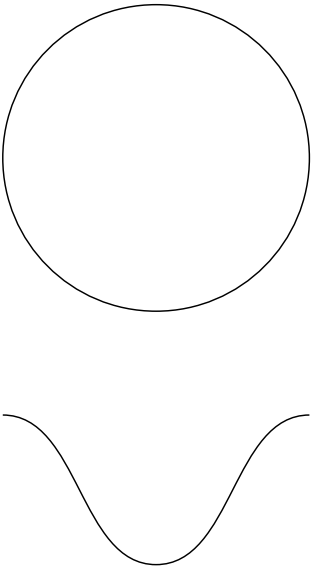

Figure 4.8 A sketch of how a hole in the road is modelled. The top shape is as seen from above, and the bottom shape is a cross section.

In order to find out how deep the radar beam reaches for a hold in the road, the cross section of a hole in the road is described with the function $f_{\text{road cross section}}(x)$:

$$f_{\text{road cross section}}(x) = \frac{d}{2}\left(\sin\left(\frac{2\pi(x-c)}{w} - \frac{\pi}{2}\right) - 1\right) \tag{4.6}$$

where x is a point on the ground surface, d is the depth of the ditch, c is the location of the center of the ditch, and w the width of the ditch. A ditch with a diameter of 0.3 meters and depth of 0.3 meters is considered necessary to avoid, and therefore necessary to detect. The corresponding plot for a hole with this specification with the center at $x = 0$ meters can be seen in figure 4.9.

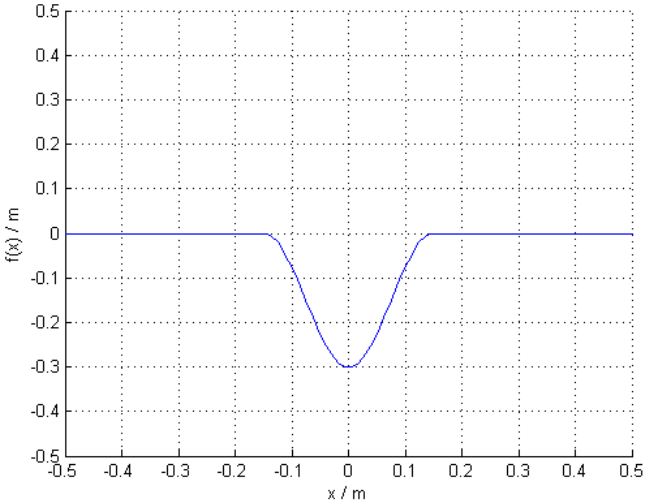

Figure 4.9 Equation 4.6 plotted with $d = 0.3$ meters, $w = 0.3$ meter, and $c = 0.0$ meters.

The maximum depth a radar beam can reach in the specified hole is then numerically calculated by finding the first intersecting point between equation 4.6 with the specified depth, width, and center, and lines from the point $y = 2.75$ (Δz of the left radar) with an increasing x, representing the truck moving forward. See figure 4.10 for an example of the numerical calculation.

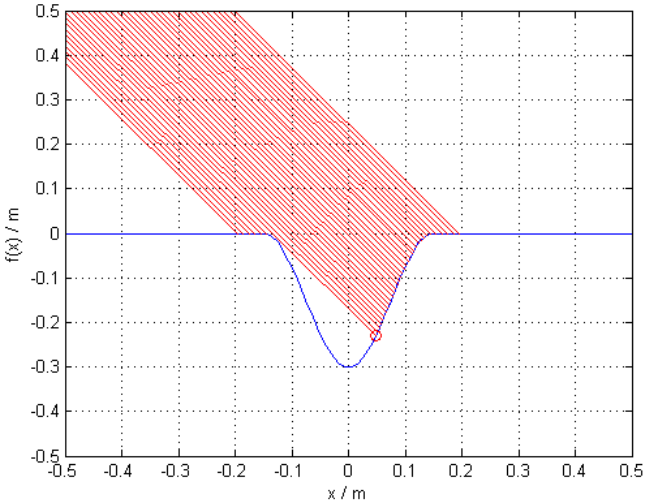

Figure 4.10 The intersections between a hole in the road with depth 0.3 meters and width 0.3 meters, and the radar beam with a length of 3.5 meters. The circle indicates the maximum depth reached by the radar beam.

The results of the calculations can be seen in figure 4.11. It is shown that the depth reached by the radar beam quickly decreases as R increases, indicating that a low R is desired. Exactly how low R that is desired depends on how precise the measurements are. The small dent at $R = 4.7$ meters can be explained by numerical errors.

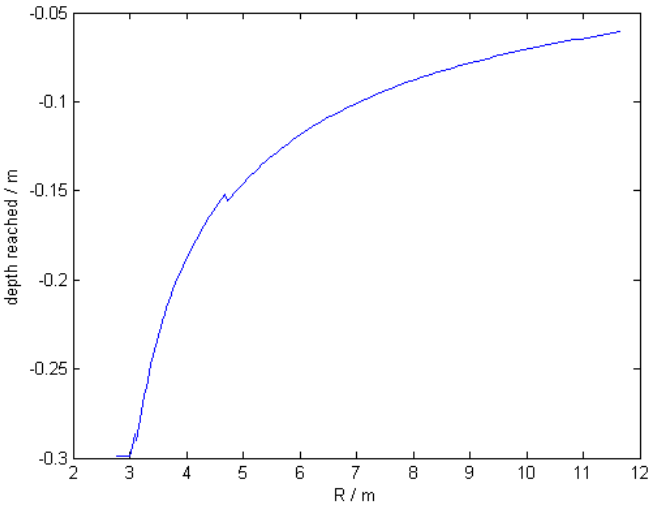

Figure 4.11 The maximum depth reached by radar beams with different length, *R*, in a hole with width 0.3 meters and depth 0.3 meters.

Ditches next to the Road

A ditch next to the road is another common object that requires accurate mapping. The difficulty is the same as for a hole in the road - the radar beam needs to be able to reach a certain depth, see section 4.1. The geometry however is different - a ditch next to the road runs along the road with the depth modelled as a sine function, see figure 4.12 for a visual description.

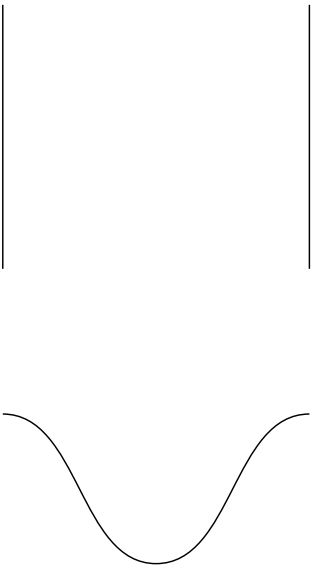

Figure 4.12 A sketch of how a ditch next to the road is modelled. The top shape is as seen from above, and the bottom shape is a cross section.

A ditch is modelled in a similar way to the hole in the road using equation 4.6. A ditch is commonly larger, and is located besides the road. This means that merely the relation between the depth reached by the radar beam and the distance between the radar beam and the ground can not be analyzed. Instead the maximum depth for different roll, pitch, and yaw angles are calculated for a ditch with depth 0.5 meter, width 0.5 meter, and center 1.75 meter to the side of the truck. An example of a numerical calculation can be seen in figure 4.13.

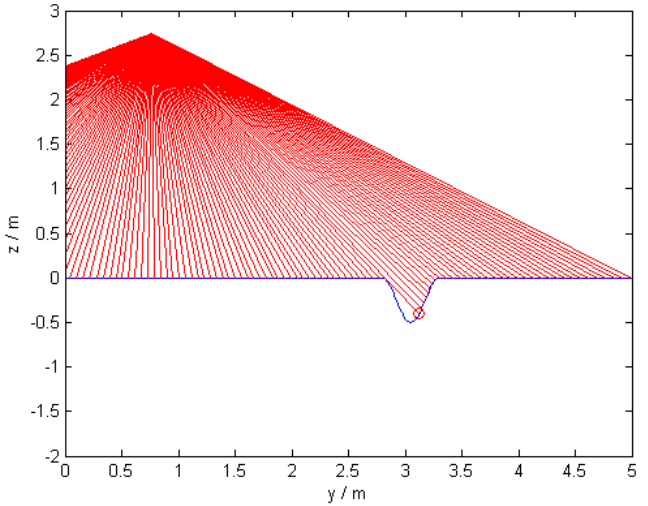

Figure 4.13 The intersections between a ditch next to the road with depth 0.5 meters and width 0.5 meters, when the radar is mounted with a roll angle of 10°, pitch angle of -30°, and yaw angle of 30°. The circle indicates the maximum depth reached by the radar beam.

Figure 4.13 shows that when the radar beam reaches a ditch, there will be very few detections on the wall of the ditch closest to the radar. This can be better visualized by plotting the y value of the detections and setting the z values to zero, see figure 4.14. Fewer detections could cause a problem when using the detections for mapping.

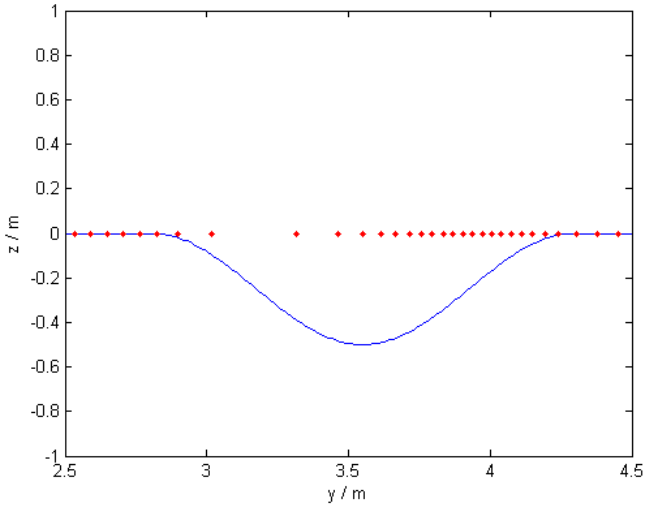

Figure 4.14 The detections in a ditch next to the road, where the z values are set to zero. The red points thus shows the distance between the radar detections in a ditch. The ditch has a depth of 0.5 meters and width of 0.5 meters, and the radar is mounted with a roll angle of 10°, pitch angle of -30°, and yaw angle of 30°.

The results for different roll, pitch, and yaw angles in figure 4.15, 4.16, and 4.17 respectively. When not varied, roll is arbitrarily set to 10°, pitch to -30°, and yaw to 30°. For these calculations, radar beams with R larger than 85 meters are not included.

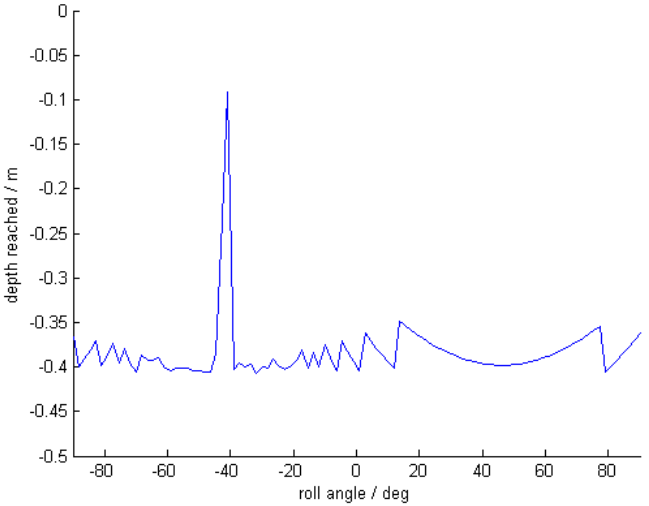

Figure 4.15 The maximum depth reached by radar beams where the radar is mounted with different roll angles, in a ditch 1.75 meters beside the truck with width 0.5 meters and depth 0.5 meters. The pitch angle is set to -30° and yaw angle to 30°.

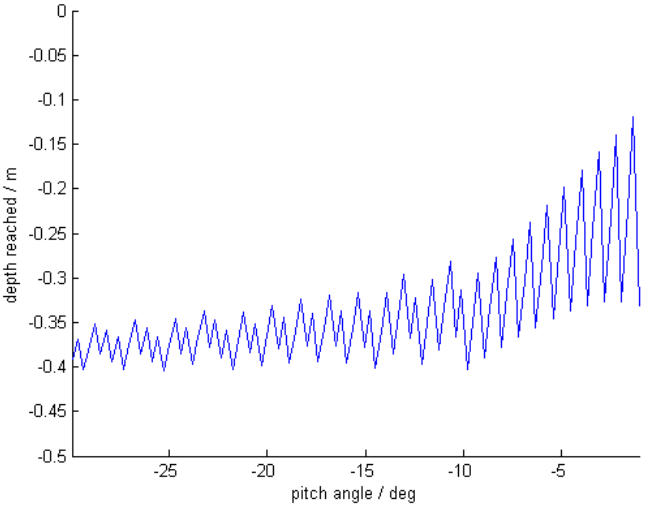

Figure 4.16 The maximum depth reached by radar beams where the radar is mounted with different pitch angles, in a ditch 1.75 meters beside the truck with width 0.5 meters and depth 0.5 meters. The roll angle is set to 10° and yaw angle to 30°.

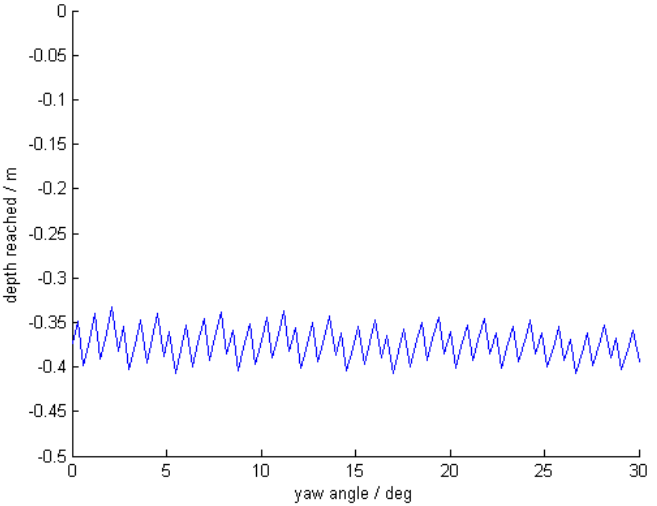

Figure 4.17 The maximum depth reached by radar beams where the radar is mounted with different yaw angles, in a ditch 1.75 meters beside the truck with width 0.5 meters and depth 0.5 meters. The roll angle is set to 10° and pitch angle to -30°.

The variations in the depth reached is likely caused by numerical errors. The general trend, however, is that the depth reached is not very dependent on the roll and yaw angles, but decreases with the pitch angle, meaning that a low pitch is desired. When the pitch reaches -10° the depth reached decreases quickly.

4.2 Radar Orientation

With the focus of this project being on detecting ditches, it is of higher importance to detect negative objects than positive objects. A low roll and pitch is therefore chosen in order to correctly detect the negative objects, and to obtain more reflections. The yaw is chosen to aim the radars to the side of the truck. See section 4.1 for details of the properties of the different radar orientations. The chosen radar orientation is shown in table 4.2. Note that this is for the left radar, and the roll and yaw will change sign for the right radar.

Angle	Value
roll	5°
pitch	-45°
yaw	30°

Table 4.2 A viable radar orientation for mapping negative objects. The values are for the left radar, and will change sign for the right radar.

When attempting to adjust the radars to the desired orientation, it was shown that the radar mount made it impossible for the radars to obtain the orientation. The radars were then adjusted as closely as possible to the desired orientation, and the results are shown in table 4.3. An illustration of the radar beams propagation from the radars to the ground ($z = 0$) can be seen in figure 4.18.

Angle	Value left radar	Value right radar
roll	11°	-8°
pitch	-33°	-27°
yaw	27°	-18°

Table 4.3 The radar angles used in the experiment.

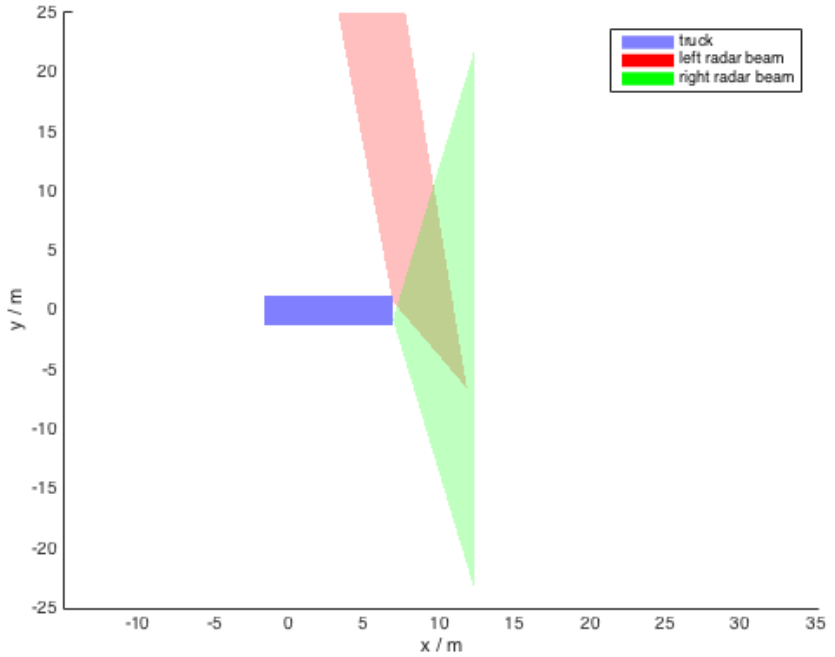

Figure 4.18 And illustration of the truck and the radar beams propagation from the radars to the ground with the angles used in the experiment. The blue square shows the truck, the red area on top the left radar beam, and the green area on the bottom the right radar beam.

4.3 Radar Position and Angle Measurements

When the radars are mounted, it is important to correctly measure their orientation and position. The measurement devices available in this project are simple mechanical measurement tools, see figure 4.19. To measure the position of the radars on the truck, a measurement tape was used.

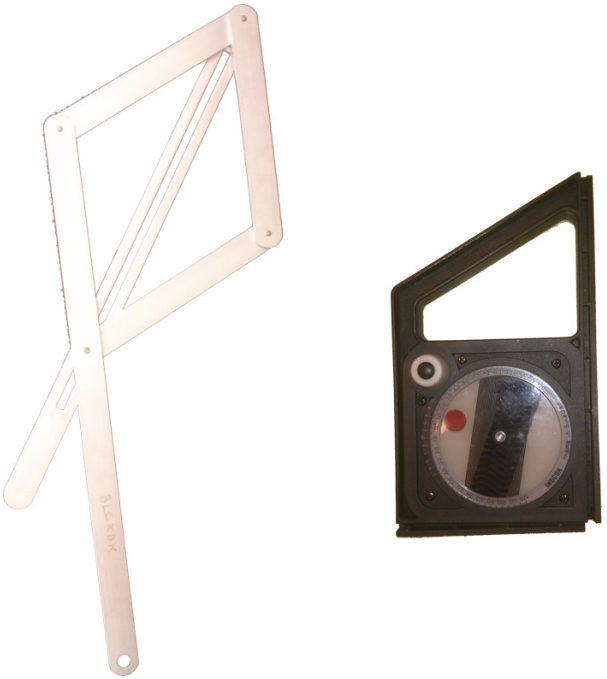

Figure 4.19 The measuring tools used to measure the radar orientations.

The inaccuracy of the measurement tools introduce another source of error, and the standard deviation of the angle measurement, $\sigma_{\text{angle meas.}}$, is arbitrarily approximated to be 1°, and the standard deviation of the position measurement, $\sigma_{\text{pos. meas.}}$, to be 0.05 meters. The standard deviations are included in table 2.4 in section 2.3.

4.4 Sampling Limitations

When the truck is travelling with a certain velocity, there will be a distance between each radar sample. The distance is calculated as the distance travelled during the sampling time at the current velocity.

$$d_{\text{sampling}} = v \cdot t_{\text{sampling}} \tag{4.7}$$

The maximal velocity is assumed to be 50 km/h, and the sampling time of the radars are 50 ms. Inserting these values in equation 4.7 gives the sampling distance

$$d_{\text{sampling worst case}} = \frac{50}{3.6} \cdot 50 \cdot 10^{-3} \approx 0.7 \text{ m} \tag{4.8}$$

A way to decrease distance between samples could be to aim the radars strategically. If the distance between the scans from the two radars would be 0.35 meters at ground level, the sampling distance would be cut in half for a velocity of 50 km/h. However, the radars in this project are not synchronized, and the data is acquired at practically random times, making it impossible to predictably reduce the sampling distance.

4.5 Test Track

The experiment is done by driving the truck in an area with known obstacles while logging the data from the sensors. The chosen area is within the Scania area in Södertälje, and a map showing the terrain, the most significant objects, and the driven route can be seen in figure 4.20, and a photograph of the terrain can be seen in figure 4.21.

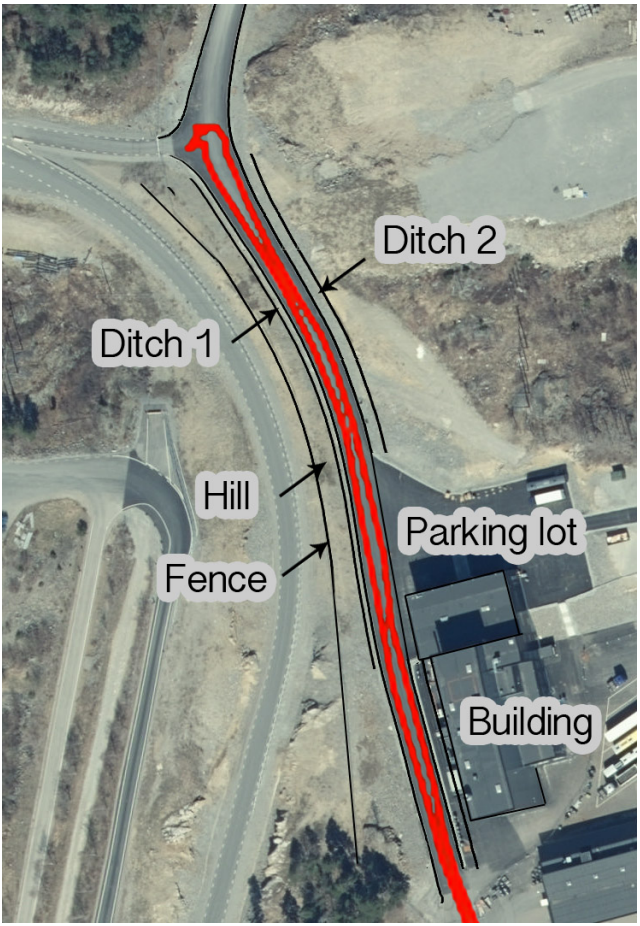

Figure 4.20 The map of the area surrounding the driven route in the experiment, and the significant objects. The path on the road indicates where the truck has driven in the experiment. © Lantmäteriet i2014/00579

Figure 4.21 A photograph of the terrain. The ditch to the left is named Ditch 1 in figure 4.21, and the ditch to the right is Ditch 2. © Scania CV AB

The measurements of the significant obstacles varies throughout the course. Ditch 1 is approximately 0.5-1.0 meter deep and 1-2 meters wide, and Ditch 2 is 0.5 meter deep and 1-2 meters wide. The hill is a few meters high, and the fence a bit over 2 meters. The altitude of the road also varies thoughout the course.

Ditch Analysis

It is of interest to see how deep into the ditches it is possible to see with the radar angles used. The same method as in section 4.1 was used to numerically calculate the depth a radar beam reaches in a ditch with width 1.5 meter and depth 1 meter, located 1 meter beside the truck. The potential difference in z caused by the unknown horizontal was calculated in the same way but with pitch set to $\pm 5^\circ$ was also calculated. Additionally, the standard deviation for each vertical angle θ was calculated according to section 3.3. The standard deviations for the radar mount angles and measurements were used. As the HPIG values are not included in the beam simulation, their standard deviations are not included. The results for the left radar can be seen in figure 4.22, and for the right radar in figure 4.23.

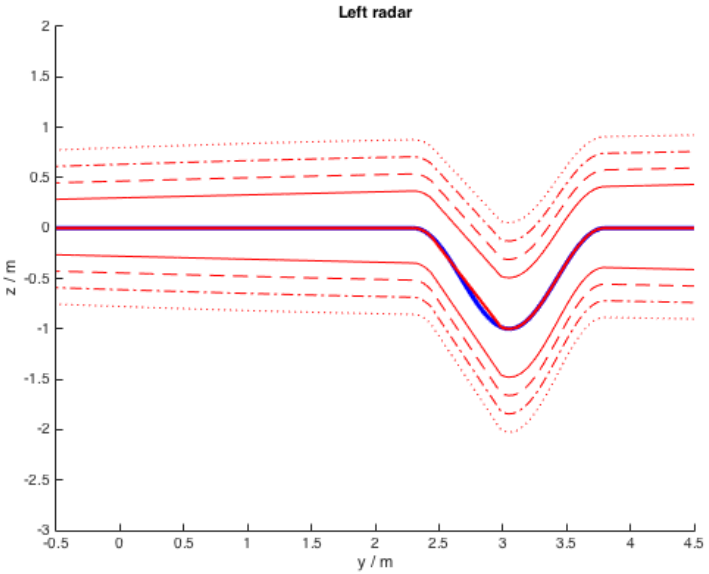

Figure 4.22 The depth reached by the left radar beam with the mounting angles used in the experiment. The thick blue line shows the ditch geometry, and the thick red line the depth reached by the radar beam; the thin, full-drawn red lines show the potential difference caused by the unknown vertical position; the dashed, dash-dot-dashed, and dotted red lines show the potential difference caused by one, two, and three standard deviations respectively.

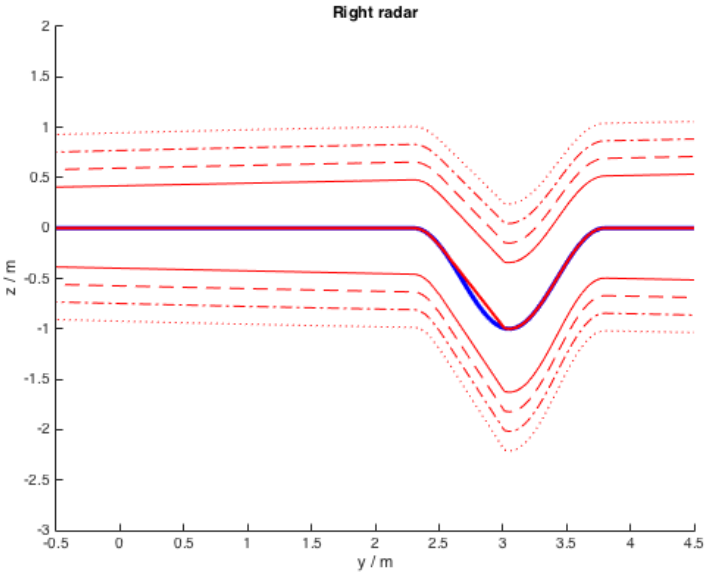

Figure 4.23 The depth reached by the right radar beam with the mounting angles used in the experiment. The thick blue line shows the ditch geometry, and the thick red line the depth reached by the radar beam; the thin, full-drawn red lines show the potential difference caused by the unknown vertical position; the dashed, dash-dot-dashed, and dotted red lines show the potential difference caused by one, two, and three standard deviations respectively.

It can be seen that the potential deviation is high, and a detection can appear to be above ground level when it is in fact from the bottom of a one meter deep ditch. This can potentially be reduced by several detections close together.

5

Results

This chapter contains the results of the experiment and the processed data according to chapter 3. At first the number of detections from the radars are analyzed, followed by the standard deviation caused by measurements, and uncertainty caused by the unknown vertical position of the detections. The velocity calculation and filter performance is then evaluated. Finally the elevation maps created from the radar and lidar data are compared, as well as the standard deviation and number of detections in each square in the radar elevation map.

5.1 Radar Detections

As the information possible to extract from the radar data directly depends on the number of targets detected by the radars, it is important to analyze the number of detections. The detections from the left and right radars are shown in figure 5.1 and 5.2 below.

The mean number of detections from the left radar is 11.0 per sample, and the mean number of detections from the right radar is 5.2 per sample, out of a maximum of 64.

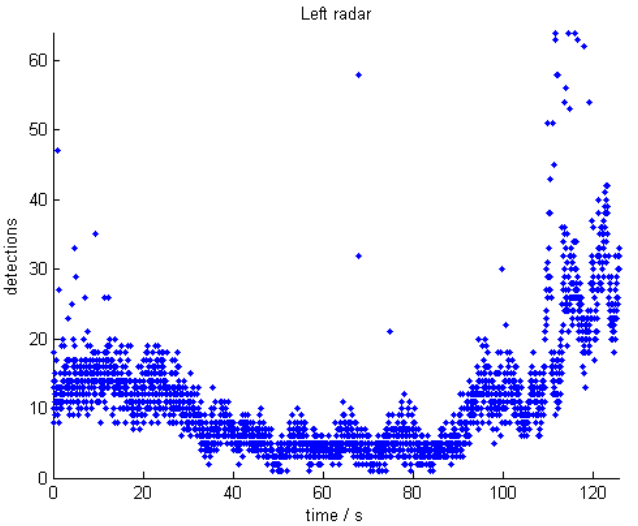

Figure 5.1 The number of detections from the left radar for each sample.

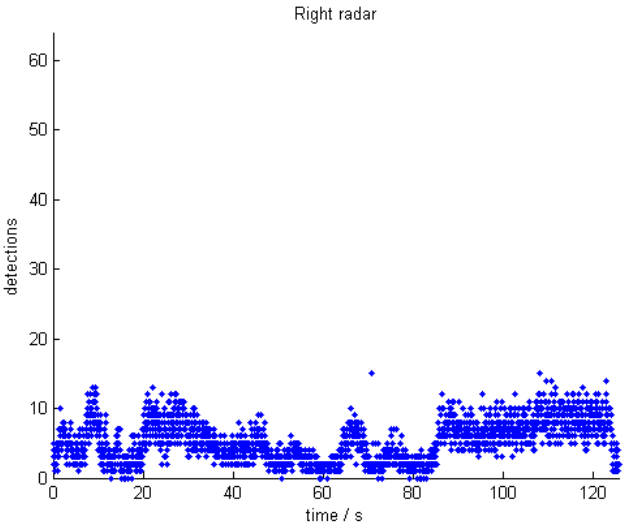

Figure 5.2 The number of detections from the right radar for each sample.

5.2 Measurement Uncertainty

Each position contains a standard deviation, which depends on the standard deviation of all measurements involved in calculating the position. These standard deviations includes the standard deviations of the radar measurements, the HPIG measurements, and the measurement of the radar position and orientation on the truck. The details of how the standard deviations were calculated can be found in section 3.3, and the result can be seen in figure 5.3.

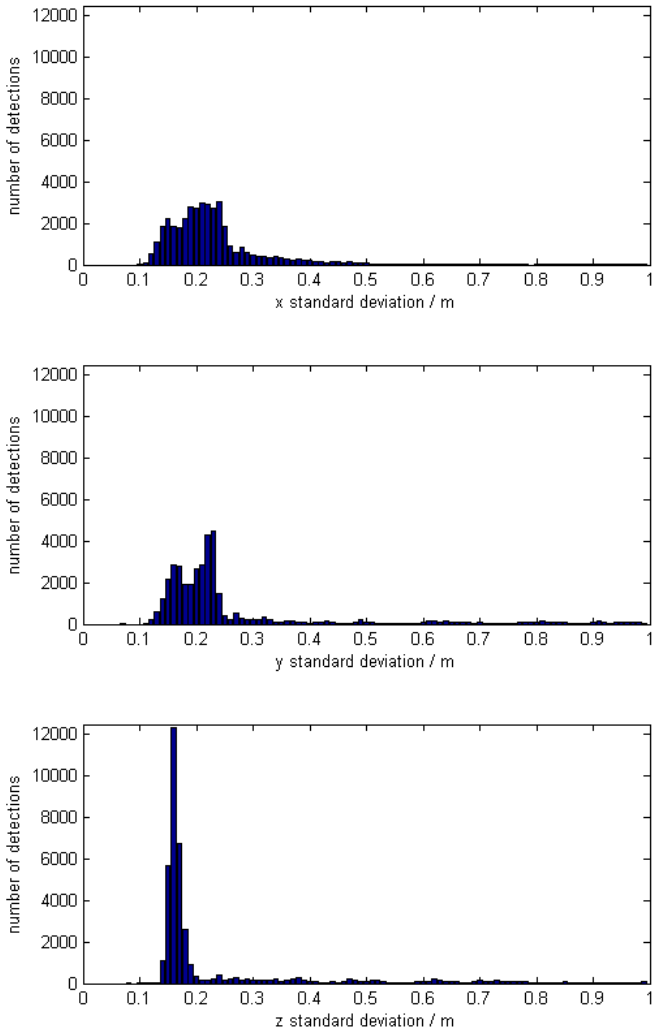

Figure 5.3 The distibution of standard deviation in global x, y, and z for the radar measurements.

It can be seen that most standard deviations for x are close to 0.2 meters, for y 0.2

meters, and for z 0.17 meters. As shown in table 3.1, 68.27% of the measurements should fall within one standard deviation of the measured position, and 95.45% of the measurements should fall within two standard deviations, and 99.73% of the measurements should fall within three standard deviations. This means that the total deviation in three dimensions

$$\sqrt{x^2 + y^2 + z^2}$$

for three standard deviations is

$$\sqrt{(3 \cdot 0.2)^2 + (3 \cdot 0.2)^2 + (3 \cdot 0.17)^2} = 0.99 \text{ meters}$$

This deviation is quite high, but could be reduced if there are several detections within a small area.

Another source of deviation is the unknown vertical angle, see section 2.3. By setting the vertical angle, $\theta_{\text{radar vertical}}$ in equation 3.8, to $\pm 5^\circ$ and finding the maximum deviation form when the vertical angle is zero, the deviation is obtained. The maximum deviation for each detection can be seen in figure 5.4.

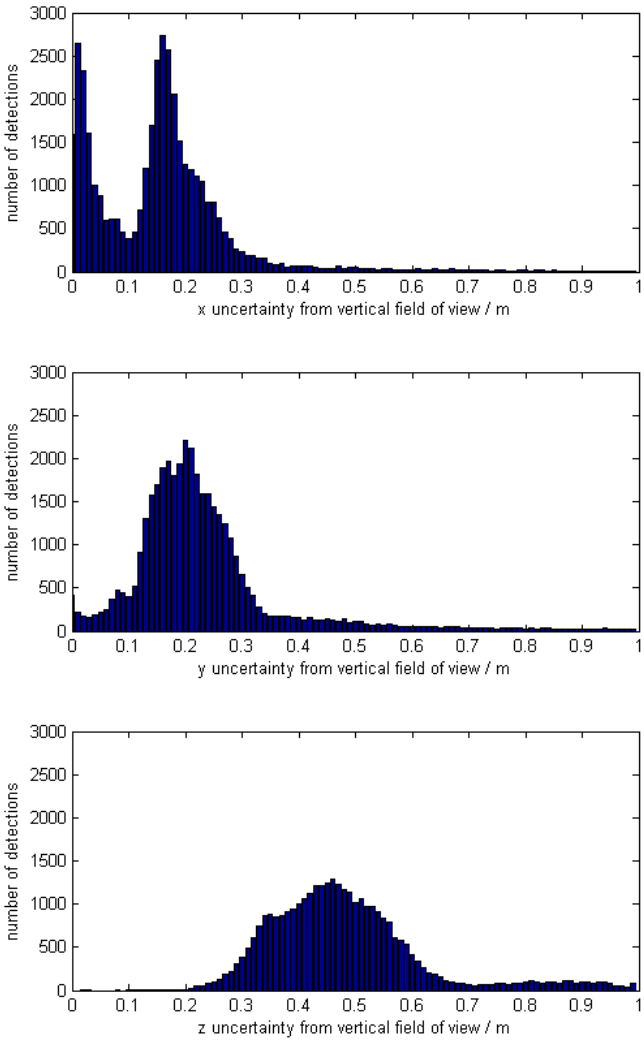

Figure 5.4 The distibution of uncertainty caused by the unknown vertical field of view in global x, y, and z for the radar measurements.

It can be seen that most uncertainties for x and z are close to 0.2, which is about the

same as for one standard deviation in the both dimensions. The uncertainty for z is however higher, and most uncertainties are close to 0.45. The total uncertainty in three dimensions is then

$$\sqrt{0.2^2 + 0.2^2 + 0.45^2} = 0.5315 \text{ meters}$$

This uncertainty is lower than that caused by the standard deviations for the measurements, but can not be reduced if several detections are within a small area.

5.3 Filter

The filter attempts to remove false detections, mostly interference between the both radar systems and double bounces. This is done by removing detections with a velocity, range, or angle higher than a specified value, see section 3.4 for details about the filter.

The global velocities of the detected objects are calculated according to section 3.2, and the results can be seen in figure 5.5, and 5.6 contains a more zoomed in plot. The distribution of the velocities can be seen in figure 5.7, and 5.8 contains a more zoomed in plot.

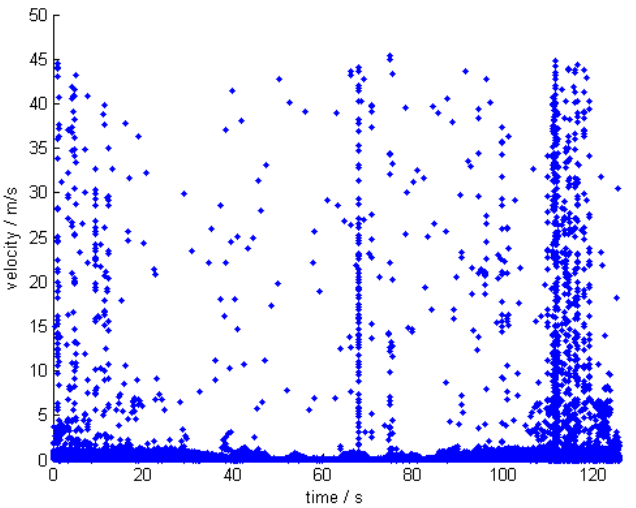

Figure 5.5 The calculated global velocity of each radar detection.

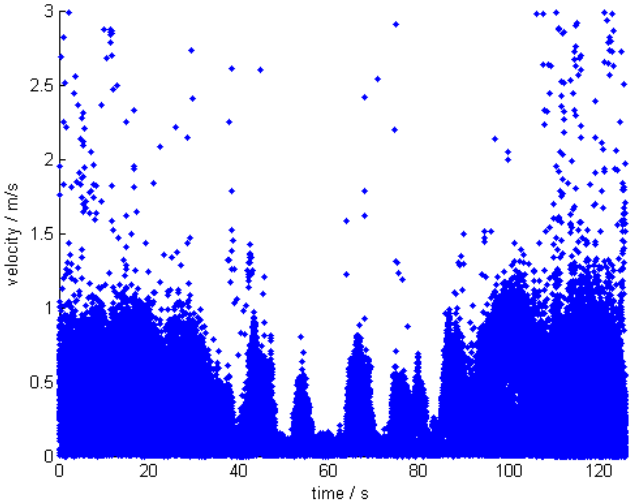

Figure 5.6 The calculated global velocity of each radar detection.

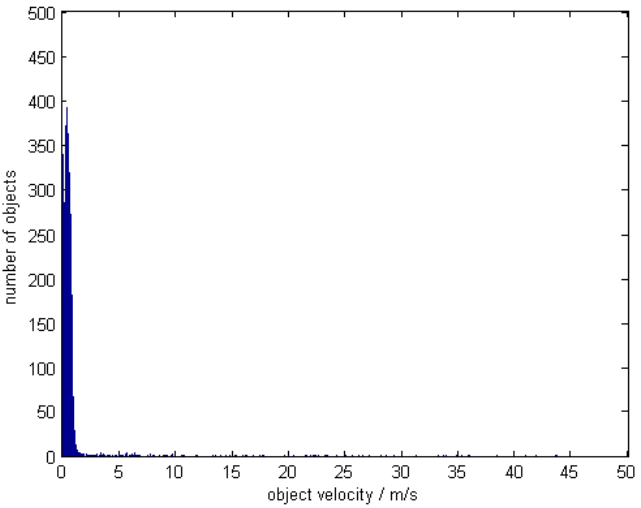

Figure 5.7 The distribution of the object velocities.

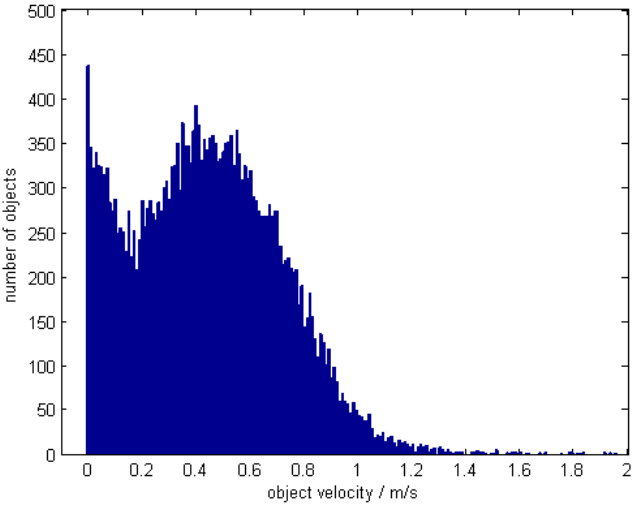

Figure 5.8 The distribution of the object velocities.

It can be seen that there are a few objects with a very high velocity. These are almost certainlty false detections. Many objects appear to have a velocity of 0-1 meter per second, which might be caused by the quantities measured by the HPIG and the approximated altitude velocity of the truck. The apparent peak at around 0.5 meters per second might be caused by the unknown vertical position of each detection, if the signal processing in the radar for example prioritizes the detection of moving objects. The result is deemed good enough to filter out false detections, but not to find the vertical position of objects detected by the radars.

The maximum velocity of the filter, v_{limit}, is set to 1.5 m/s, and the minimum and maximum range and horizontal angle are listed in table 2.3. The number of detections removed by the filter in each sample can be seen in figure 5.9 for the left radar, and figure 5.10 for the right radar.

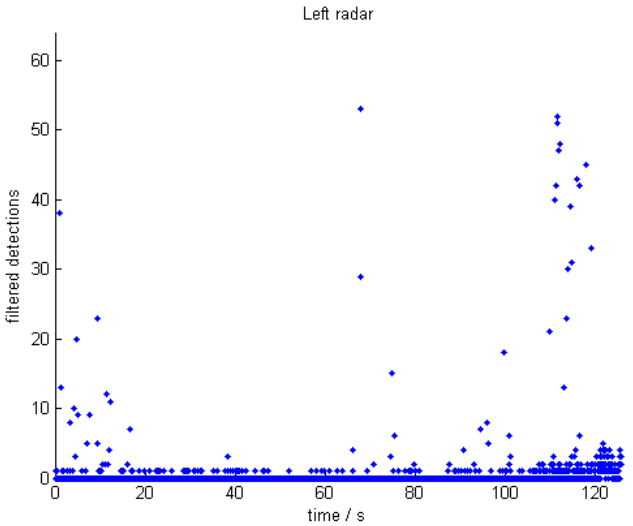

Figure 5.9 The number of detections removed by the filter for each sample for the left radar.

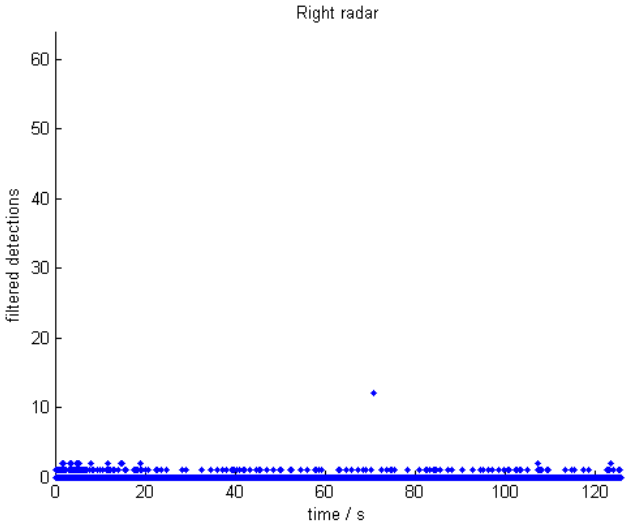

Figure 5.10 The number of filtereddetections removed by the filter for each sample for the right radar.

The average number of filtered detections per sample is 0.54 for the left radar, and 0.10 for the right radar. This accounts for 5 % and 2 % respectively. These are low numbers, indicating that most detections are good.

5.4 Elevation Map

The elevation map, along with a map showing the number of detections within each square, and one showing the standard deviation for the detections within each square, are created according to section 3.5. The square size is arbitrarily set to 0.5^2 m^2, which is small enough to give a detailed map, and large enough to not contain too many holes caused by no radar detection. The map is visualized as a surface where the color represents the elevation of each square.

Comparison with Terrain Map

The radar elevation map is first compared with the terrain described in section 4.5. The elevation map with the terrain obstacles overlaid can be seen in figure 5.11.

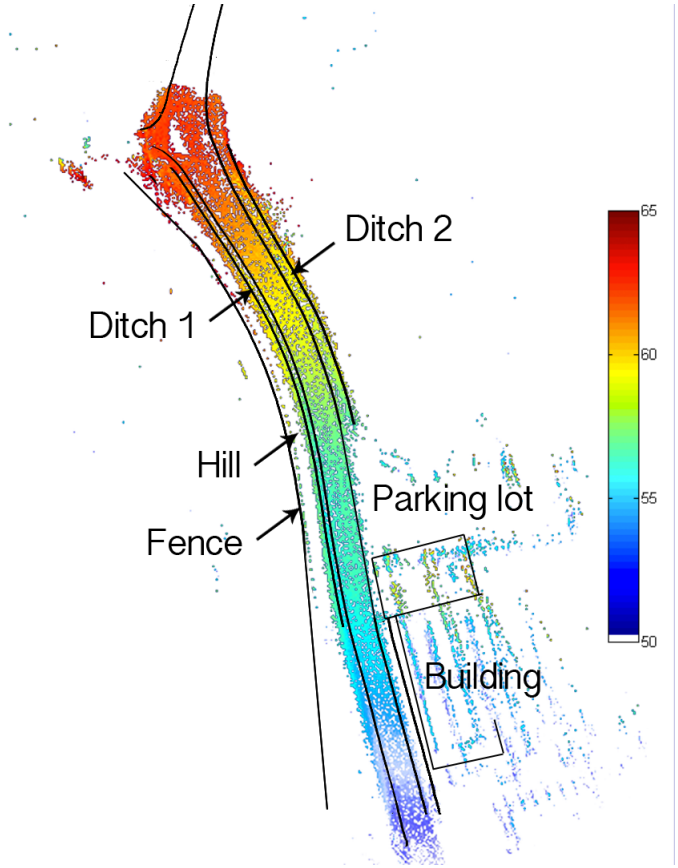

Figure 5.11 Radar elevation map with significant objects marked. Each square represents the terrain in a 0.5^2 m^2 area, and the color shows the elevation in each square. The colorbar shows the elevation in meters above mean sea level.

It can be seen that there are several detections inside the building. Since the detecions appear as lines with equal distance between them, it is likely that the detections inside the building are caused by double bounces of the radar beams.
Since it is difficult to see how well the map represents the terrain, the map is zoomed in on the area between the Ditch 1 and Ditch 2 labels in figure 5.11. The zoomed in elevation map along with the objects overlaid can be seen in figure 5.12.

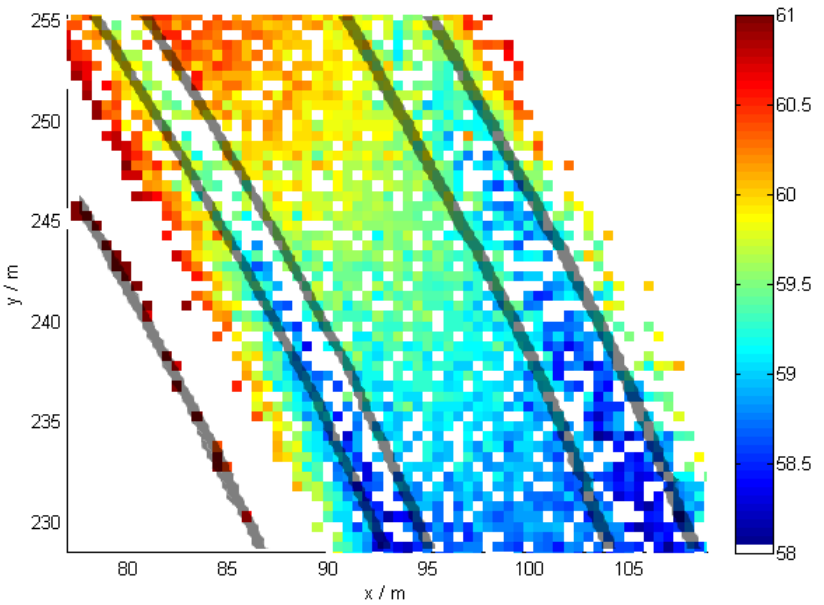

Figure 5.12 Zoomed radar elevation map with significant objects marked. Each square represents the terrain in a 0.5^2 m^2 area, and the color shows the elevation in each square. The colorbar shows the elevation in meters above mean sea level.

It can be seen that the ditches are clearly visible, and have approximately the correct dimensions. As predicted in section 4.1, there are fewer detections on the side of the ditch closest to the radars.

Comparison with Lidar Map

In order to quantitatively find out how well the radars can map the environment, a lidar map was created in the same way as the radar map. The lidar map can be seen in figure 5.13.

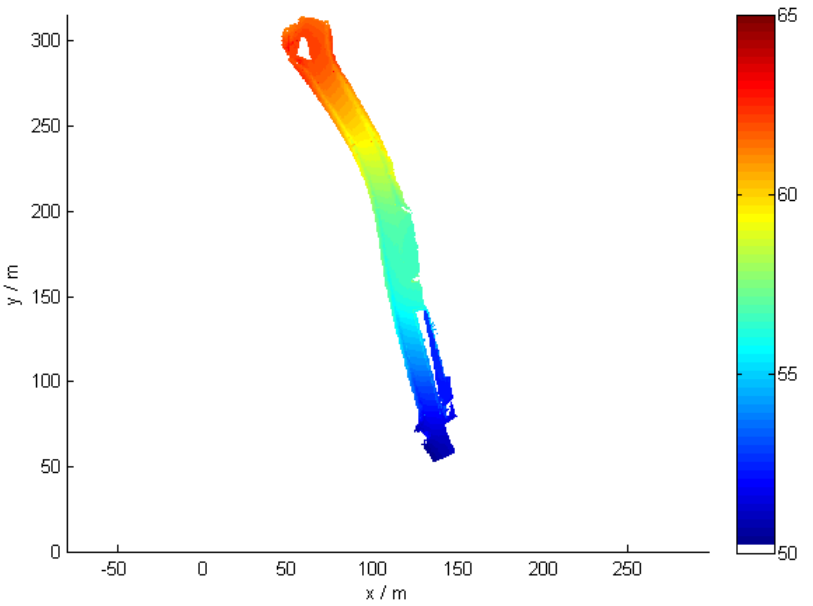

Figure 5.13 Lidar elevation map. The colorbar shows the elevation in meters above mean sea level.

The lidar map appear to be very dense, and contains very few squares without detections in the vicinity of the road. By calculating how many squares that have one or more detections in the lidar map, but do not have any detections in the radar map, it is be found that the radar map fills 83 % of the lidar map.
It is difficult to compare the two maps, so the same are as in figure 5.12 is zoomed in upon. See figure 5.14 for the zoomed in radar map, and figure 5.15 for the zoomed in lidar map.

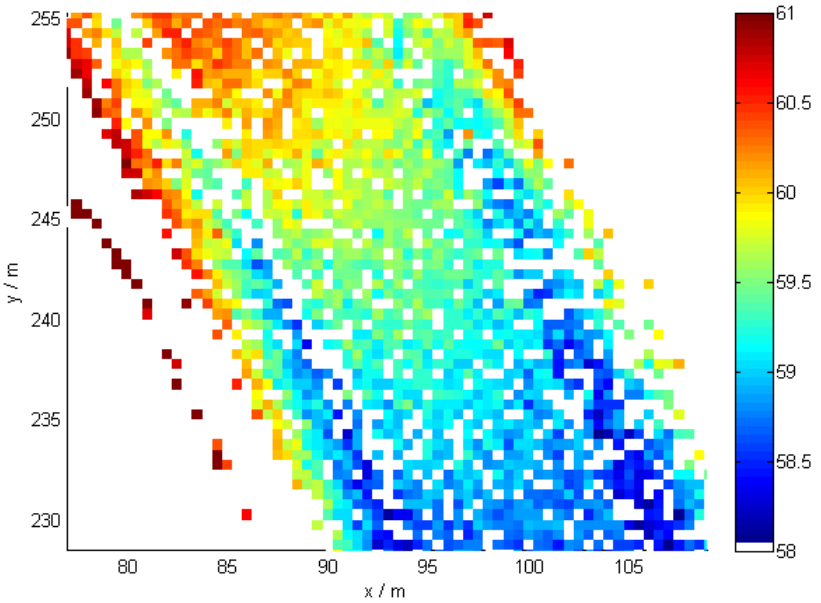

Figure 5.14 Zoomed radar elevation map. The colorbar shows the elevation in meters above mean sea level.

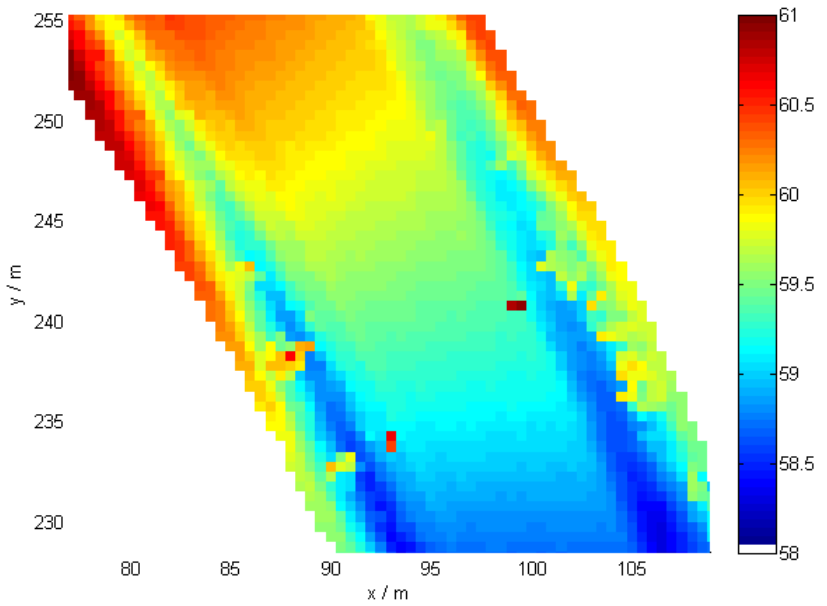

Figure 5.15 Zoomed lidar elevation map. The colorbar shows the elevation in meters above mean sea level.

It is clearly shown that the ditches are visible in both elevation maps, and that the general elevation is very similar. Some positive objects which appears on the lidar map are however not present in the radar map. The positive objects are most likely metal poles, grass, and bushes.

By creating a map where each square is the radar elevation minus the lidar elevation, the difference between the two maps are clearly shown. This map is shown in figure 5.16.

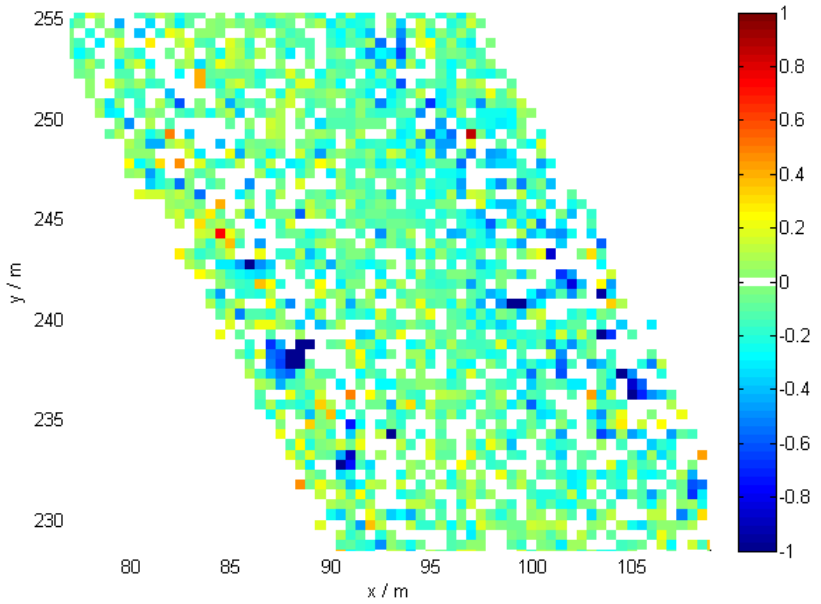

Figure 5.16 The radar elevation minus the lidar elevation map. The colorbar shows the elevation difference in meters.

Similarly to what was seen previously, the radar do not properly map the smaller positive objects. Besides that, the deviation is quite evenly spread out, as expected.

By calculating this difference between all squares in the map in figure 5.16, the difference distribution is shown in figure 5.17. This is only done in squares which are filled in both maps.

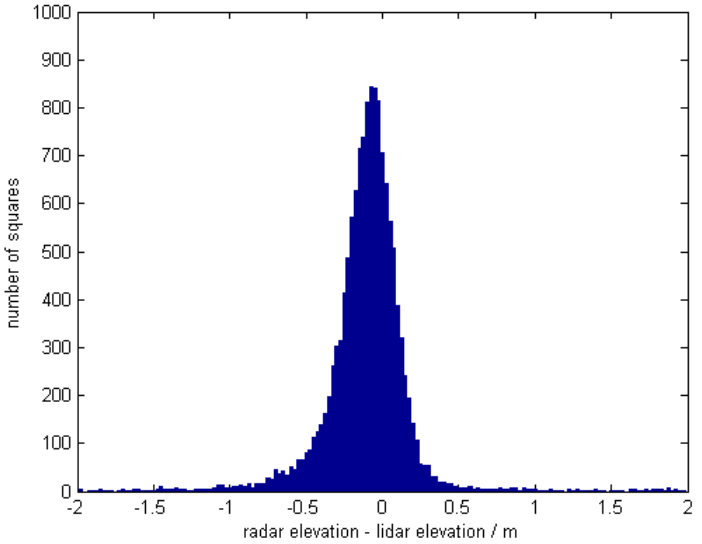

Figure 5.17 The distribution of the radar elevation minus the lidar elevation for every square which is filled in both maps.

The deviation is centered around zero, but with a slight offset. As with the velocity, the offset might be caused by the unknown vertical position of each detection, if the signal processing in the radar for example prioritizes the detection of moving objects. and the most detections in the radar map fall within 0.5 meters of the lidar map. There are a few deviations with greater deviation, which possibly are the small positive objects not detected by the radars.

Standard Deviation and Count

In order to analyze how much each square can be trusted, the standard deviation and number of detections within each square are calculated.The number of detections in each square can be seen in figure 5.18, and a zoomed in part of the map in figure 5.19.

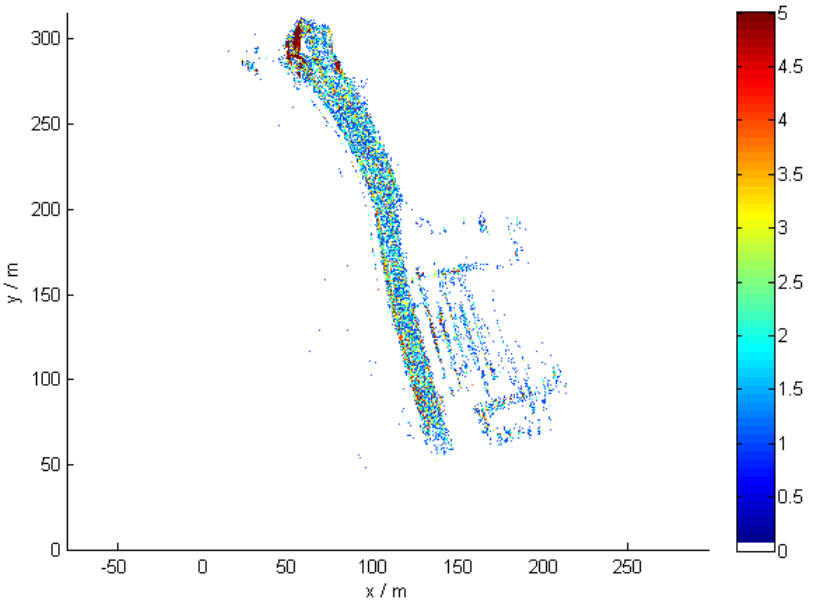

Figure 5.18 Number of detections in each square in the radar elevation map. The colorbar shows the number of detections.

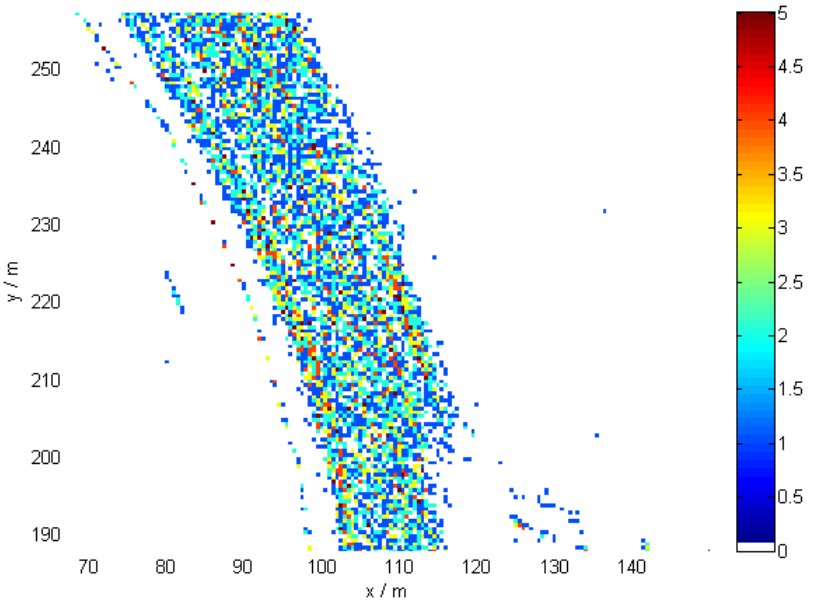

Figure 5.19 Number of detections in each square in the radar elevation map. The colorbar shows the number of detections.

It can be seen that most squares contain 1-2 detections, with a few containing more. The distribution of the number of detections in each square can be seen in figure 5.20.

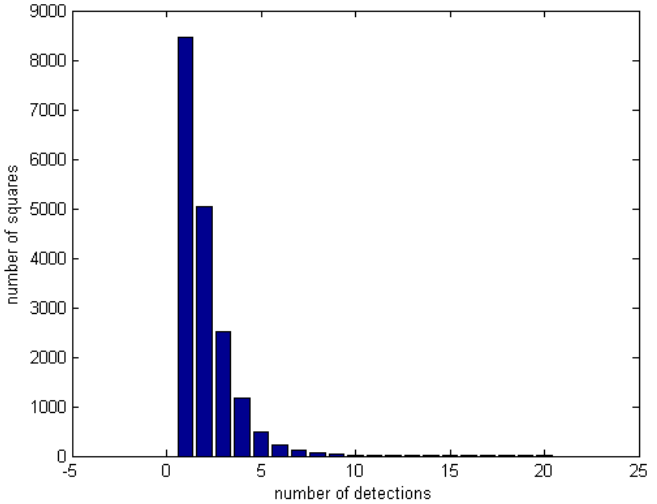

Figure 5.20 The distribution of the number of detections in each square.

The standard deviation of each square is calculated according to equation 3.26, and the resulting map can be seen in figure 5.21. A zoomed in part of the map can be seen in figure 5.22.

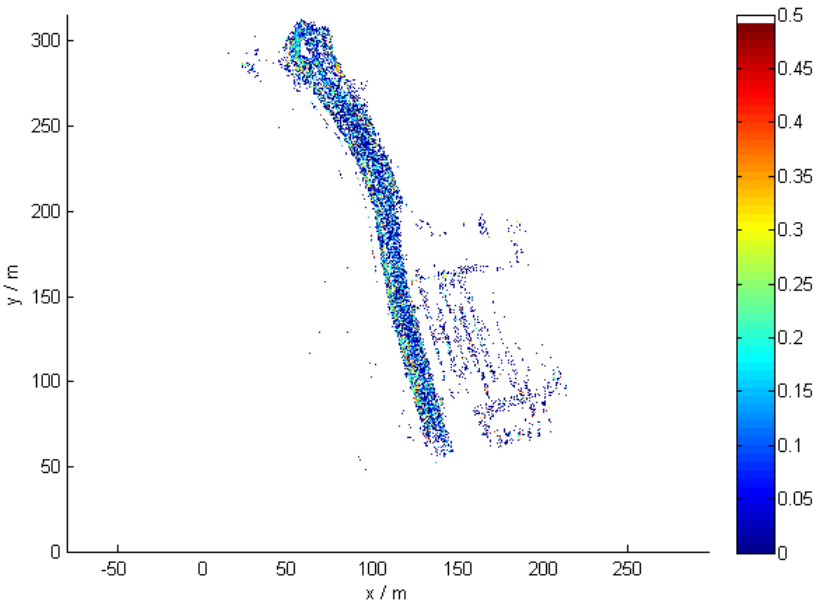

Figure 5.21 Standard deviation for the radar elevation map. The colorbar shows the standard deviation in meters.

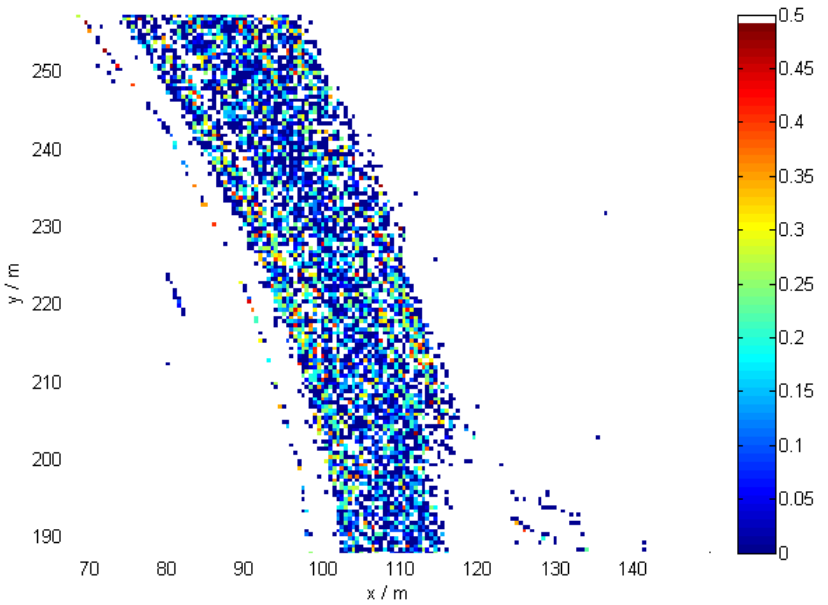

Figure 5.22 Standard deviation for the radar elevation map. The colorbar shows the standard deviation in meters.

The standard deviations appear to be low, most close to zero. The large amount of standard deviations at zero is probably caused by the large amount of squares with only one detection. The standard deviations seem to be evenly spread out, as expected. The large standard deviations seem to be on the small hills next to the ditches. This is as expected, since the detections in one square can have very different elevation depending on where on the hill it is comming from. The distributin of the standard deviations can be seen in figure 5.23.

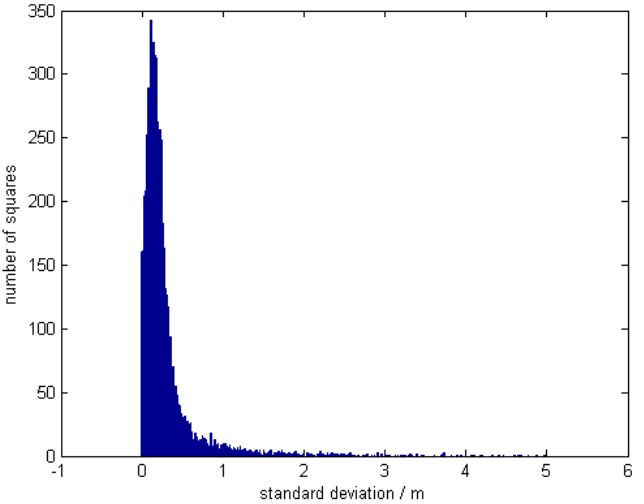

Figure 5.23 The distribution of the standard deviations in each square.

As previously seen, most standard deviations are very low and close to zero. The larger ones are most likely from squares with a large difference in elevation.

6

Conclusions

This chapter contains the conclusions drawn from the results - how well the elevation mapping works, and how it can be improved.

As the detections carry the information about the environment, it is vital to retrieve as many detections as possible. There are many factors that will determine how many detections that will be retrieved by the radar, such as the angle of incidence and the reflectivity of the surface. As discussed in section 4.4, the distance between each sample is 0.7 meters when driving at a velocity of 50 km/h. If there is no detection at a certain point, the distance will be twice as much in that area. The number of detections were presented in section 5.1. The number of detections are very low compared to the maximum number of detections per sample (64). In particular the number of detections from the right radar at only 8% of the maximal value, whereas the left radar had 17%. This is likely due to the high angle of incidence, which is larger for the right radar. There were many reflections from the building, even when taking the double-bounces into consideration. The building is orthogonal to the ground, creating a lower angle of incidence. This incidates that a lower pitch angle for the radars would generate more detections, which in turn would create a denser and more reliable map. The result of the low number of detections can be seen in section 5.4, where it is presented that the radar map is filled to 83% of the lidar map. This is a decent amount, and can possibly be filled to a higher degree if driving through the area more times. Section 5.4 presents the number of detections for each square in the radar elevation map, and it can be seen that most squares only have one to three detections. This makes the map both less reliable and accurate than a map with a higher density of detections.

In order to properly filter out bad detections, it is important to be able to calculate the velocity of the objects with a high accuracy. Most targets are expected to have a velocity of zero, with a deviation of less than 0.5 meters per second caused by the different vertical position of the target. The bad detections, caused by interference with the other radar and double bounces, are expected to have a higher velocity. As seen in section 5.3, the calculated range velocity appear to be

very high, with a number of detections close to 1 meter per second. This is likely caused by the dynamics of the truck cab, the internal filters of the HPIG, and the crudely calculated altitude velocity. As future work, a Kalman filter could be used to obtain a more accurate altitude velocity. The filter do remove several detections with a very high velocity, which are most likely intereference. As can be seen in the radar elevation map in section 5.4, there are also several appearent double bounces present, which indicates that a more advanced filter needs to be used.

The resulting elevation map created from the radar data is decently accurate, which can be seen in section 5.4. The ditches appear to be correctly mapped, both when compared to the measured terrain and the elevation map created by the lidar. There are however some deviations between the radar and lidar map, but the elevation of most squares in the radar map fall within 0.5 meters of the corresponding square in the lidar map. The radar do however appear to miss small objects, like a metal pole visible in the lidar map. This might improve with a higher number of detections per sample, as more information would be retrieved.

The standard deviation of a square in the elevation map shows how much the detections varies. A high standard deviation could indicate a high uncertainty in the detections, but also that the elevation difference in that area is high. Section 5.4 shows the standard deviations of the detections in each square. While the vast majority of squares has a standard deviation of less than 0.5 meters, which is quite high. There is also a considerable amount of squares with a higher standard deviation. The figures shows that the standard deviations are high in the squares where the terrain elevation differs the most, which is as expected.

In order to determine if the deviations in the elevation map are within the teoretical limits, the potential deviations caused by the measurement standard deviation and unknown vertical position were calculated for each detection, see section 5.2. The results show that the potential deviations can be a bit over one meter. The uncertainty caused by measurement standard deviations could be reduced with more detections in each square if a more sophisticated mapping algorithm were to be used.

The uncertainty caused by the unknown vertical position could be reduced by a large amount if the global velocity of objects were to be accurately calculated. The current method for calculating the velocity results in quite large errors, as seen in section 5.3. The cause of the errors are likely the filtered values from the HPIG and the unknown altitude velocity, which could both possibly be fixed by a more advanced model of the velocity without adding any extra sensors.

In order to improve the accuracy of the elevation map, an possibly make it more detailed by using smaller squares, a larger number of detections needs to be ob-

tained. This is probably possible by decreasing the pitch angle of the radars, which would need a custom mount. A custom mount could also decrease the uncertainties in the radar mount angles. A second important improvement would be to correctly find the vertical position of the radar detections. As discussed, this could be done if the velocity were to be accurately mapped, but a radar which provides the vertical angle of the detection could also be a solution, albeit a possibly more expensive one.

Bibliography

Agnew, D. (2014). *Negative obstacle detection with stereo camera and long range radar*.
http://www.google.com/patents/US20140168001.
Accessed: 2015-05-24.

Cheng, H. (2011). *Autonomous Intelligent Vehicles*. London: Springer.

Diebel, J. (2006). *Representing attitude: euler angles, unit quaternions, and rotation vectors*.

Dutch, S. (2014). *The universal transverse mercator system*.
https://www.uwgb.edu/dutchs/FieldMethods/UTMSystem.htm.
Accessed: 2015-05-24.

Forward, S. (2008). *Driving Violations: Investigating Forms of Irrational Rationality*. Uppsala: Universitetsbiblioteket.

Jain, V. and P. Heydari (2012). *Automotive Radar Sensors in Silicon Technologies*. Springer New York.

Jaynes, E. T. (2003). *Probability Theory - The Logic of Science*. New York: Cambridge University Press.

Ku, H. H. (1966). "Notes on the use of propagation of error formulas". *Journal of Research of the National Bureau of Standards*, pp. 263 –273.

Levanon, N. and E. Mozeson (2004). *Radar Signals*. Wiley.

Marcu, F. M. (2009). *Semiactive Cab Suspension Control for Semitruck Applications*. Blacksburg, Virginia.

Melvin, W. L. and J. A. Scheer (2013). *Principles of Modern Radar Vol. II: Advanced Techniques*. Edison, NJ: Scitech Publishing.

Mittskus, A. and J. Lux (2006). "Detecting negative obstacles by use of radar". *NASA Tech Briefs, November*, pp. 14–16.

Mostafa, M. M. and J. Hutton (2001). "Direct positioning and orientation systems: how do they work? what is the attainable accuracy". In: *Proceedings, The American Society of Photogrammetry and Remote Sensing Annual Meeting, St. Louis, MO, USA, April*, pp. 23–27.

Ozguner, U., T. Acarman, and K. Redmill (2011). *Autonomous Ground Vehicles*. Artech House.

Rabinovich, S. G. (2005). *Measurement Errors and Uncertainties, Third Edition*. New York: Springer.

Shaw, A. (2013). *Accelerating Sustainability: Demonstrating the Benefits of Transportation Technology*. Intelligent Transportation Society of America.

Skolnik, M. I. (2008). *Radar Handbook, Third Edition*. McGraw-Hill.

Teknomo, K. (2006). *Recursive average and variance*. http://people.revoledu.com/kardi/tutorial/RecursiveStatistic/index.htm. Accessed: 2015-04-13.

European Commission (2014). *EU Transport in Figures - Statistical Pocketbook*. Luxembourg: Publications Office of the European Union.

Vlacic, L. (2009). *Intelligent Vehicle Technologies*. Elsevier Science & Technology Books.

Xu, G. (2007). *GPS: Theory, Algorithms and Applications*. Springer Berlin Heidelberg.

Lund University
Department of Automatic Control
Box 118
SE-221 00 Lund Sweden

Document name
MASTER´S THESIS

Date of issue
June 2015

Document Number
ISRN LUTFD2/TFRT--5970--SE

Author(s)
Christopher Dahlin Rodin

Supervisor
Bo Bernhardsson, Dept. of Automatic Control, Lund University, Sweden
Anders Rantzer, Dept. of Automatic Control, Lund University, Sweden (examiner)

Sponsoring organization

Title and subtitle

Radar Based Estimation of Ditches in the Vicinity of the Road

Abstract

Radars used for detecting objects with a positive elevation, such as other vehicles, are common in autonomous parking and braking systems in modern vehicles. Detecting objects with a negative elevation, such as ditches and holes, is however more troublesome. A common approach is to use a lidar, but a lidar is very costly and fragile compared to a radar. In this thesis, two two-dimensional radars are attached above the windshield of a truck and aimed down towards the ground.

At first the geometrical limitations of detecting ditches is analyzed in order to find which mounting angles of the radars are viable. Data is then collected from the radars, with the determined angles, a Global Positioning System (GPS) unit, and Inertial Measurement Unit (IMU) by driving the truck in a real world terrain. Data from a lidar is also recorded for reference.

Combined with a GPS and IMU, the radar detections are first transformed from the radar coordinate system, the a truck coordinate system, and finally to global Universal Transverse Mercator (UTM) coordinates. The global position of each detection is filtered, and finally used to create an elevation map of the environment. A similar map is also created from the lidar detections.

The resulting radar elevation map accurately maps the terrain near the vicinity, including the ditches next to the road. The radars appear to miss small objects, and the density of the detections is quite low for the radar mount angles used.

In order to improve the accuracy, the vertical position of the radar detection needs to be determined. A higher density of detections would also improve the mapping, which could be aquired by decreasing the pitch angle of the radars.

Keywords

Classification system and/or index terms (if any)

Supplementary bibliographical information

ISSN and key title
0280-5316

ISBN

Language
English

Number of pages
1-92

Recipient's notes

Security classification

http://www.control.lth.se/publications/